ORIGINAL ARTICLE

Case study for a performance based rapid seismic assessment methodology (PERA2019) based on actual earthquake damages

Hasan Huseyin Aydogdu[1] · Alper Ilki[2]

Abstract

Most of the buildings in Turkey constructed before 1999 Kocaeli and Duzce Earthquakes do not have sufficient seismic resistance due to construction errors and do not satisfy the recent Turkish Building Earthquake Code (2018) or its preceding versions. In Istanbul, the building stock consists of 1,116,300 buildings. Clearly, seismic safety assessment of this amount of buildings is not practically possible by code-based detailed assessment approaches, which generally assess the seismic performance of buildings in terms of pass or fail, rather than rank and classify/prioritize these buildings considering their seismic safety. Moreover, the probability of a catastrophic earthquake that could hit Istanbul is high. Therefore, to minimize casualties and economic losses, it is important to determine the most vulnerable existing buildings effectively in terms of cost and duration. Accordingly, Istanbul Metropolitan Municipality has started to evaluate the seismic safety of existing reinforced concrete buildings using the PERA2019 method considering the actual structural data collected on site. The buildings are then divided into 5 seismic risk classes from low-risk to very high-risk according to the computed seismic safety ratio. In this study, the reliability of the PERA2019 is evaluated by considering the predicted risk classes of another large group of actual buildings that have been subjected to actual earthquakes and experienced earthquake-induced damages in different extents. The comparative evaluation of actual seismic damages and predictions of PERA2019 showed clearly that the methodology has a sound ability to estimate the structural seismic performance of the investigated buildings.

Keywords Building stock · Rapid seismic assessment · Reinforced concrete buildings · Resilience · Earthquake damages · Sub-standard

✉ Hasan Huseyin Aydogdu
  aydogduha@itu.edu.tr

  Alper Ilki
  ailki@itu.edu.tr

[1] Earthquake Engineering Program, Istanbul Technical University, Istanbul, Turkey

[2] Faculty of Civil Engineering, Istanbul Technical University, 34469 Maslak, Istanbul, Turkey

1 Introduction

Turkey has suffered from devastating earthquakes in the past. The experience of previous earthquakes shows that the buildings in seismically active regions in Turkey are extremely prone to heavy damage or collapse (Bibbee et al. 2000; Holzer et al. 2000; Scawthorn and Johnson 2000; Ozmen 2000; Erdik 2001; Bruneau 2001; Celep et al. 2011; Tapan et al. 2013). After the heavy losses of the 1999 Marmara Earthquakes, a common seismic awareness has arisen in Turkey, and the year 2000 has been accepted as a milestone (Ilki and Kumbasar 2000; Ozdemir et al. 2002). Although there has always been an up-to-date seismic design code in force in Turkey since 1940s, most of the existing buildings built before the year 2000 have been constructed improperly without complying with the seismic code regulations and original design projects, with poor quality materials and workmanship, and incorrect structural details. Deterioration of these poorly constructed buildings over time, mostly because of damages due to corrosion of reinforcing bars, further magnifies the problem (Inci et al. 2013).

These relatively old, sub-standard and deteriorated buildings must be assessed urgently in terms of their potential seismic performance in order to take necessary measures in a rationally prioritized approach to minimize losses against future earthquakes. On the other hand, conducting a widespread code-based detailed evaluation for such a high number of buildings is inefficient both in terms of cost and time, if not impossible. To reduce this huge problem to a manageable scale, a simplified and economical, yet reliable and realistic rapid seismic assessment method is needed for planning intervention strategies in a rational and prioritized way. However, current seismic regulations such as Provisions for the Seismic Risk Evaluation of Existing RC Buildings under Urban Renewal Law (2019) and Turkish Building Earthquake Code (2018) do not involve a building-based ranking/prioritization system, but they rather lead decisions as pass or fail (i.e. risky or not, providing life safety or not). A usual structural engineering investigation of the existing buildings in Istanbul according to the current seismic regulations will probably end up with the fact that almost every ordinary building constructed before the year 2000 is risky (or they will not satisfy life safety-controlled damage performance target). Therefore, making use of a reliable and rapid seismic performance ranking procedure for individual buildings is a key issue for prioritizing buildings with respect to their seismic risks. Sorting the buildings by their seismic capacity to demand ratios is a reasonable way to fill this gap. Actually, in some countries that are in active seismic regions, important steps have recently been taken towards such a categorization. In New Zealand, SLaMA, a new risk-based methodology for intervening earthquake-prone buildings has been published (NZSEE 2017). The procedure divides buildings into six risk classes in terms of the New Building Standard% (NBS%). D and E Class buildings with a NBS% less than 1/3, have to be intervened to reach at least 2/3 NBS level. The allowed time window to mitigate the seismic risk of the building changes with the seismicity of the region and the importance/function of the building. Gentile et. al. (2019) performed a validation study to investigate the accuracy of the SLaMA procedure via comparison with pushover analysis on 40 RC frames. As the probability of a catastrophic earthquake that could hit Istanbul is very high in the near future (Parsons et al. 2000), it is gravely important to identify the most vulnerable existing buildings and prioritize them according to their seismic risks to minimize losses. The evaluation and prioritization of earthquake-prone buildings according to their seismic performance were studied by various researchers. Sextos et al. (2007) proposed a combined pre and post-earthquake assessment approach with a GIS-integrated system. The pre-earthquake assessment method is based on street survey applications. Marasco et al. (2021) introduced a simplified procedure

with a surrogated model for large-scale building stocks, and the authors performed a valida-tion study through nonlinear finite element models.

According to Cakti et al. (2019), the building stock in Istanbul consists of 1,116,300 build-ings, and 194,000 of them will be subjected to moderate, heavy or very heavy damage after a Mw = 7.5 scenario earthquake. The code-based detailed evaluation of over 1 million build-ings cannot respond to the urgency of risk mitigation studies in Istanbul. Thus, the aim of the rapid seismic methodology that is assessed in this study is to find those buildings with a cost and time-effective yet sufficiently accurate approach. Istanbul Metropolitan Municipal-ity has started a rapid and cost/time-efficient seismic assessment campaign in Istanbul. In the scope of this project, the Municipality evaluated nearly 25,000 sub-standard reinforced con-crete buildings using PERA2019 method (Ilki et al. 2021a) and ranked them by their seismic risk level from low risk to very high risk (Aydogdu et al. 2023b). Detailed performance-based assessment efforts are saved for high and very-high risky buildings to reduce the scale of risk mitigation studies and increase the feasibility of the process. Currently, the Municipality has also started a campaign aiming to retrofit thousands of buildings starting from very high risky ones determined through the PERA2019 methodology.The good agreement of the used rapid assessment methodology with the detailed seismic safety assessment results obtained based on the Provisions for the Seismic Risk Evaluation of Existing RC Buildings under Urban Renewal Law (2019) and Turkish Building Earthquake Code (2018) through three-dimen-sional structural analyses was already presented by Aydogdu et al. (2023a) before. In the same study, the reliability of 5 s stage assessment and 3 street survey methods were compared too, and the results showed that the PERA2019 method yielded the most compliant outputs with the code-based detailed assessment assessments, which is the consequence of the code-com-pliant algorithm of PERA2019.

The seismic performance of the buildings that were constructed before 2000 during the 2023 Kahramanmaraş earthquakes was investigated thoroughly in the disaster area by the authors several times. Most of the buildings that caused life losses were not built according to their codes and did not meet the minimum requirements of their era's seismic design codes. The lessons that were learned from the 2023 Kahramanmaraş earthquakes dictate that there is an urgency of implementing seismic performance assessment on the country scale in Turkey. Computing the seismic safety of the buildings and classifying them through an economical and time-effective yet sufficiently accurate rapid performance based analysis approach can respond to the urgency of the risk mitigation studies, so interventions can start from the build-ings containing the highest seismic risk. The proposed approach takes the deficiencies that the building stock has and the probable effects of these weaknesses into consideration. Moreover, the PERA2019 methodology has demonstrated its success on buildings that were subjected to different earthquakes, as well as code-based assessment comparisons. In this study, the reli-ability of the rapid seismic safety assessment methodology used in Istanbul (PERA2019) is evaluated through a database of actual structural seismic damages of actual buildings estab-lished based on damage survey reports prepared after earthquakes that affected different regions of Turkey (Afyon 2002; Bingöl 2003; Aegean Sea 2020).

2 PERA2019: general information on the methodology

The PERA method was initially introduced by Ilki et al. (2014) to determine the seismic performance of reinforced concrete (RC) frame buildings rapidly and reliably based on the criteria provided by Turkish Seismic Design Code (2018). The method was modified in

2019 to assure conformity with the up-to-date seismic provisions (Provisions for the Seismic Risk Evaluation of Existing RC Buildings under Urban Renewal Law 2019). The use of the modified version of the methodology is not limited to frames, but can also be applied for RC buildings with shear walls. The overall flow and background of the method have recently been summarized by Ilki et al. (2021a) and Aydogdu et al. (2023b). The method is developed for buildings up to 10-story high, for which the first mode of vibration is generally dominant. In the first step, the critical story is identified based on engineering judgment; typically the ground floor. The number of stories, plan dimensions of the stories, story heights, cross-section dimensions of the critical story columns and shear walls, locations of the columns and shear walls in the building plan, slab type and common beam cross-section dimensions, compressive strength of concrete, reinforcement type (plain/deformed) and details in terms of spacing of transverse reinforcement and the ratio of longitudinal reinforcement, irregularities in plan and elevation, reinforcement diameter loss due to corrosion and seismic demand parameters determined considering ground conditions are required to perform the analysis. A typical team consisting of a civil engineer and a technician or an architect can evaluate and finalize data collection for an ordinary building in 1.5 h on average.

The seismic capacity is determined by an incremental approach repeating the simplified structural analyses and assessment procedures at each increment of seismic demand beginning from very small seismic actions until the seismic capacity of the building is reached (Fig. 1). The incremental analysis begins with the first step, which is corresponding to 1% of the acceleration demand spectrum. If the building is not determined critical (this process is explained below), the spectral acceleration values of the spectrum are increased by 1% (such as 2%, 3%…) until the step that the building is determined critical which is the iteration step $i+1$. Then, step i is determined as the last step for which the building is not critical, and the PGA value of the spectrum applied at iteration i is defined as the PGA capacity of the building. Seismic Safety Ratio (SSR), determined through this incremental procedure is the ratio of PGA capacity to PGA demand (Eq. 1). For example, the SSR value of 50% means that the PGA capacity of the considered building is 50% of the PGA demand. If the building satisfies the PGA demand, the SSR value of that building is equal to or greater than 100%.
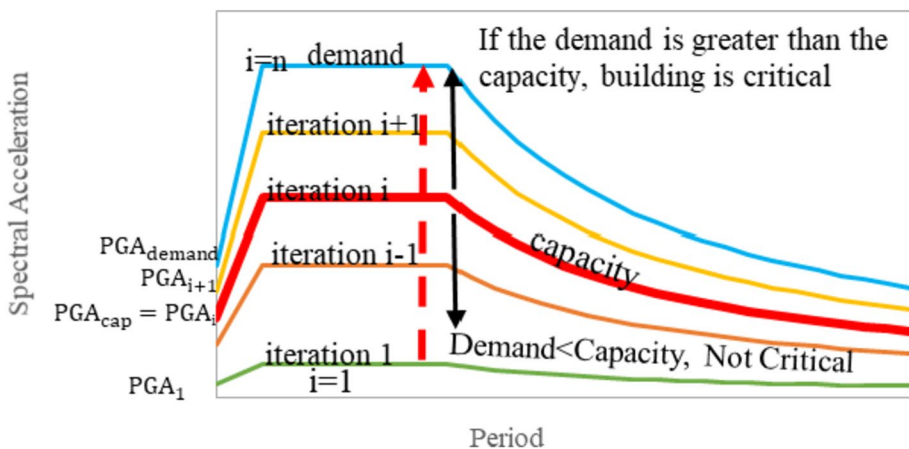

Fig. 1 Typical elastic acceleration spectra scaled at various levels for iterations

$$\text{Seismic Safety Ratio(SSR, \%)} = 100 \times \frac{PGA_{Capacity}}{PGA_{Demand}} \tag{1}$$

In the computation phase of the method, the reference limits for deciding if the building satisfies the performance target are in parallel with the Provisions for the Seismic Risk Evaluation of Existing Buildings-2019 (RBTE 2019). A validation study for the previous version of this seismic document, Provisions for the Seismic Risk Evaluation of Existing Buildings-2013 (RBTE 2013), was presented by Binici et al. (2013). The ratio of the sum of the shear forces that are carried by risky columns and shear walls (V_{risky}) to the total base shear force (V_{story}) must be calculated to determine whether the building can sustain the seismic demands considered. To determine if a vertical element is risky, these members are classified into member categories based on their confinement conditions and flexural shear loading ratios as given in Table 1. Afterwards, the columns and shear walls, which exceed either the demand/capacity or interstory drift ratio limits defined in Table 2 according to their member categories, are classified as risky members. It should be noted that the interstory drift ratio is the lateral displacement divided by the height of the considered column. The demand/capacity or interstory drift ratio limit approaches adapted from RBTE (2019) are similar to the acceptance criteria for reinforced concrete columns and shear walls defined by ASCE 41–17 (2017).

Figure 2 illustrates the computation of the global performance of the structural system. If the average axial load ratio is less than 10% at the critical story, the total shear force of the risky columns and shear walls (V_{unsafe}) are allowed up to 35% of the story shear force (V_{story}), while none of the columns and shear walls is allowed to exceed their demand/capacity ratio limits for the buildings that have average axial load ratio greater than 65%. For the cases where the average axial stress is between 10 and 65% at the critical story, interpolation should be made in order to calculate the allowed story shear limit. The normalised average axial load ratio is computed by Eq. (2).

$$S_{av} = \frac{\sum_{i=1}^{n} \frac{N_{k,i}}{A_i f_{cm}}}{n} \tag{2}$$

In the equation, S_{av} is the normalised average axial load ratio, $N_{k,i}$ is the axial load acting on vertical structural members (i.e. column or shear wall) at the critical story, A_i is the cross-sectional area of vertical member, f_{cm} is the compressive strength of the existing

Table 1 Categorization of columns and shear walls

Columns			Shear walls		
V_e/V_r	$s \leq 100$ mm, 135° hooks, $A_{sh} \geq 0.06 sb_k (f_{cm}/f_{ywm})$*	All other cases		$V_e/V_r \leq 1.0$	$1.0 \leq V_e/V_r$
$V_e/V_r \leq 0.7$	A	B	$2.0 \leq H_w/l_w$	A	B
$0.7 < V_e/V_r \leq 1.1$	B	B	$H_w/l_w > 2.0$	B	B
$1.1 < V_e/V_r$	B	C			

s: stirrup spacing, A_{sh}: cross-sectional area of transverse reinforcement, H_w: wall height, l_w: wall length

V_e: flexural shear demand, V_r: shear strength, f_{cm}: the compressive strength of the existing concrete,

f_{ywm}: the yield stress of transverse reinforcement, b_k: width of the core concrete

Table 2 Demand/capacity and interstory drift ratio limits for reinforced concrete columns and shear walls

A Class Columns

$N_K/(A_c f_{cm})$	m_{limit}	Drift(%)$_{limit}$
≤0.1	5	0.035
≥0.6	2.5	0.0125

B Class Columns

$N_K/(A_c f_{cm})$	$A_{sh}/(sb_k)$	m_{limit}	Drift(%)$_{limit}$
≤0.1	≤0.0005	2	0.01
	≥0.006	5	0.03
≥0.6	≤0.0005	1	0.005
	≥0.006	2.5	0.0075

C Class Columns

m_{limit}	Drift(%)$_{limit}$
1	0.005

A Class Shear Walls

$N_K/(A_c f_{cm})$	$V_e/(b_w d f_{cm})$	Boundary Region	m_{limit}	Drift(%)$_{limit}$
<0.1	≤0.9	Exists	6	0.03
		N/A	4	0.015
	≥1.3	Exists	3.5	0.015
		N/A	2	0.0075
>0.25	≤0.9	Exists	3.5	0.02
		N/A	2	0.01
	≥1.3	Exists	2	0.01
		N/A	1.5	0.005

B Class Shear Walls

$V_e/(b_w d f_{cm})$	m_{limit}	Drift(%)$_{limit}$
≤0.9	4	0.02
≥1.3	2	0.01

N_K, the axial load of the element; A_c, cross-sectional area of the element; m_{limit}, demand/capacity ratio limit for the element; Drift(%)$_{limit}$: allowed drift limit for the element; b_w, width of the element; f_{ctm}, the tensile strength of concrete; d, depth of the section

Fig. 2 The total allowed shear force ratio of columns exceeding their demand/capacity ratio limits. The ratio is dependent on the average axial load ratio at the critical story (V_{unsafe}: The total shear force that is carried by risky elements, V_{story}: The total shear force of the story)
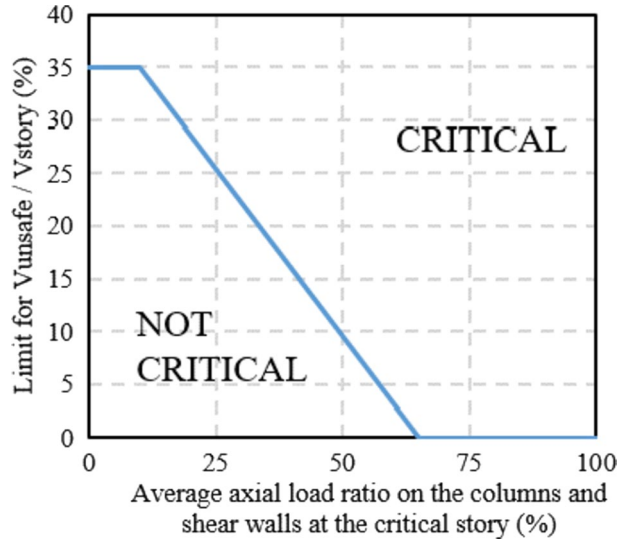
concrete and n is the total number of columns and shear walls. The axial loads on the columns and shear walls are calculated considering the tributary area of these vertical members with an assumption of 10 kN/m² and 13 kn/m² unit gravity loads for residential and public buildings respectively. The assumed gravity loads are determined by taking into account dead loads and reduced live loads. It should be noted that the definition of N_k is slightly different with respect to the definition of N_k in RBTE (2019).

Finally, the buildings in the examined region can be prioritized concerning their seismic risk levels depending on their SSR values. Building risk classes defined by Ilki et al. (2021a) are given in Table 3. As the SSR value is lower, the seismic risk of the building is higher. A similar classification approach in the SLaMa procedure (NZSEE 2017) divides buildings into six risk classes in terms of the New Building Standard% (NBS%). The buildings with an NBS% less than 1/3 have to be intervened to reach at least 2/3 NBS level according to SLaMa. A similar classification approach to New Zealand is in force In Italy. In addition, the expected annual economic loss is also a key parameter that is taken into consideration in Italy. Further information on this classification approach can be found in Di Ludovico et al. (2017), Polese et al. (2018) and Cosenza et al. (2018).

A brief summary of the general flow of PERA2019 to compute SSR value is given in Fig. 3. In this figure, the Performance Reduction Coefficient (PRC) corresponds to the cumulative multiplication of 0.9 for each structural irregularity and weakness. A more comprehensive summary of the PERA2019 methodology was explained by Ilki et al. (2021a).

Table 3 Building risk classes and risk levels corresponding to various SSR intervals for the global structural system

SSR (%)	Building risk class	Risk level
≥ 100	A	Low risk
75- < 100	B	Low risk
50- < 75	C	Medium risk
25- < 50	D	High risk
< 25	E	Very high risk

In addition to the validation study of the initial version of the PERA method (limited to frame structures), which was based on detailed analyses of 672 buildings by Ilki et al. (2014) as well as real earthquake damages of 21 buildings after the 1995 Dinar, 1999 Kocaeli, 2002 Afyon, and 2011 Van earthquakes, the reliability of the PERA2019 method (applicable for the frame and frame-shear wall buildings) has studied through a numerical study focusing on 73 existing reinforced concrete buildings by Aydogdu et al. (2023a). In that study, a good agreement was demonstrated between the SSR values of the buildings and detailed code-based (TSDC 2007; TBEC 2018; and RBTE 2019) structural seismic assessment results. The results of the numerical study presented by Aydogdu et al. (2023a)
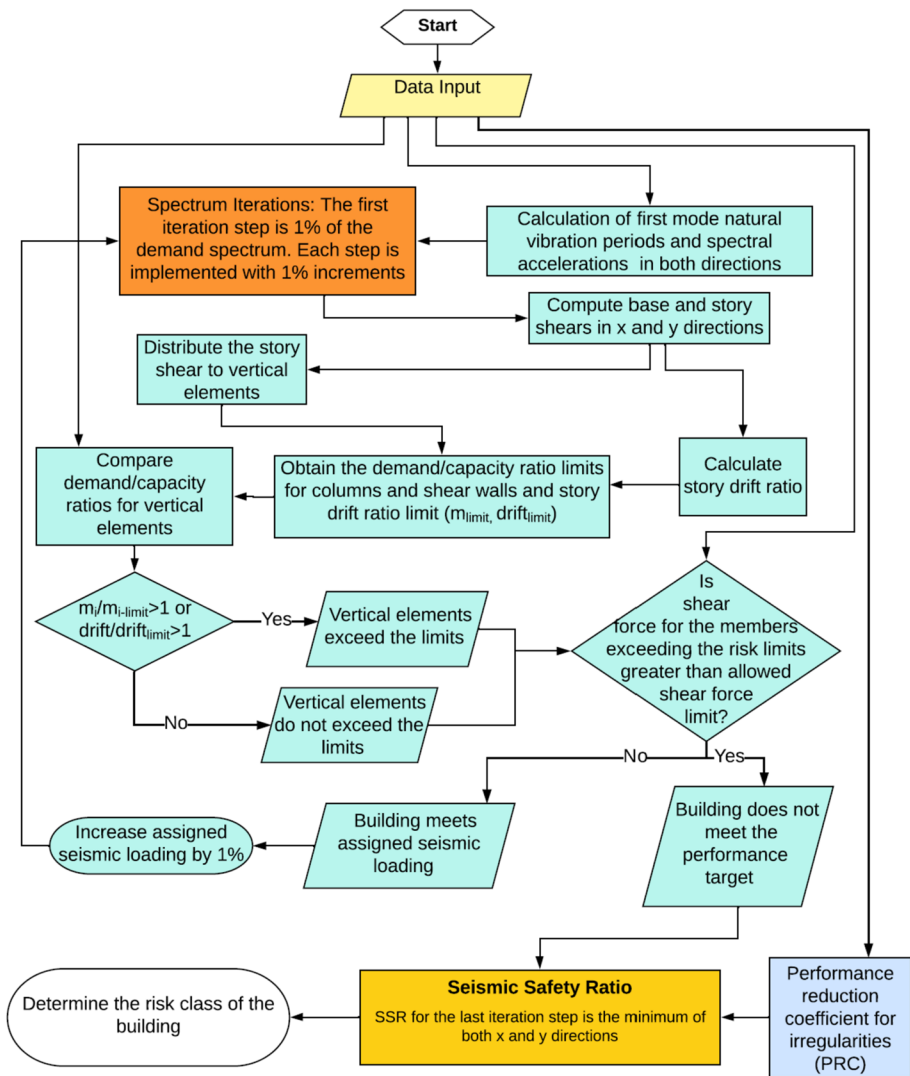

Fig. 3 A brief flowchart of the algorithm for the PERA2019 method (Aydogdu et al. 2023b). The information about input data is given in the first paragraph of this section

have demonstrated that contents of D and E risk classes of buildings as determined by the PERA2019 method capture 95% of the buildings that were found to be in collapse limit state according to detailed code-based assessment procedure (TSDC 2007; TBEC 2018; and RBTE 2019). Most of the buildings in collapse prevention or controlled damage performance according to the code-based assessment procedure were found to be in C, B or A risk classes according to predictions of the PERA2019 method (Fig. 4). Further details on the PERA2019 method can be found elsewhere (Ilki et al. 2021a).

3 Case study

One of the effective ways to examine the reliability of a seismic evaluation method is to compare the results of the method with actual earthquake-induced damages. Within the scope of this comparative study, SSR values and risk classes of 42 buildings, which were subjected to earthquake excitations in real life, are computed to examine the reliability of the methodology. Then, the damage states of the buildings are compared with the assigned risk classes through the PERA2019 method.

3.1 Buildings

The structural characteristics and damages of 18 buildings that experienced 2002 Afyon and 22 buildings that experienced 2003 Bingöl earthquakes were taken from the SERU database (METU 2003). Besides these 40 buildings with different extents of seismic damage, two buildings, which experienced the 2020 Aegean Sea Earthquake and were also investigated in this study. The structural information for the buildings located in Izmir was collected from the site directly, while the others are gathered from the SERU database of Middle East Technical University (METU 2003). The buildings in Afyon are located in 6 different districts, while the ones in Bingöl are divided into 4 regions according to their location and soil parameters. In addition, 2 buildings in Izmir are located near Karşıyaka
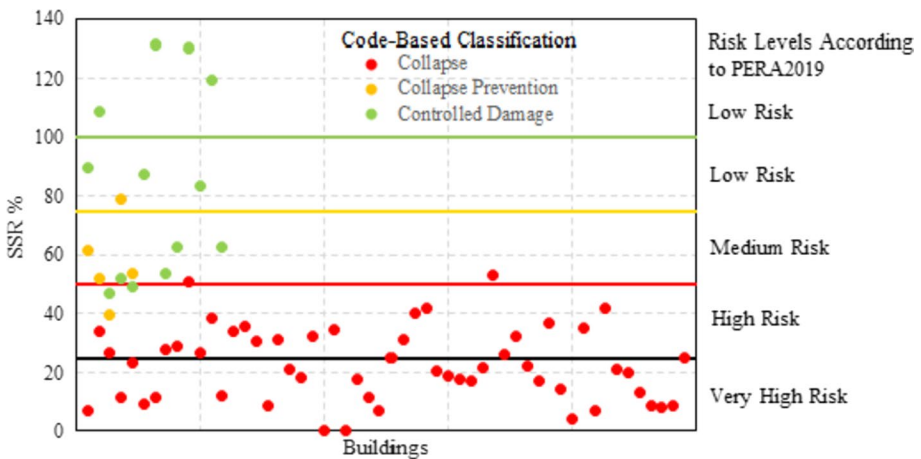

Fig. 4 Comparison of detailed assessment results with estimations of PERA2019: score scatter with risk limits (adopted from Aydogdu et al. 2023a). The horizontal axis illustrates the buildings in a random order

and Izmir stations. Figure 5 demonstrates the distribution of the number of floors, compressive strength of the existing concrete, reinforcement type and axial load ratio acting on vertical structural members of the buildings. The average compressive strength of concrete is 10 MPa and the frequency of smooth S220 type rebar is more than 90%. These distributions reflect the overall characteristics of the Turkish building stock, which have been presented by Aydogdu et al. (2023b) for Istanbul, comprehensively. The number of buildings that were built before the publication of TSDC (1998) is 29, while 13 of the evaluated buildings were built after 1998, but before the publication of the two most recent seismic design codes in Turkey, which have been published in 2007 and 2018, respectively.

Minimum requirements in various Turkish Seismic Design Codes for high-seismicity regions are given in Table 4, which demonstrates that seismic design codes in Turkey have involved most of the crucial structural details since 1975. Apparently, 98% of the evaluated buildings fail to comply with the minimum compressive strength of concrete requirements of all seismic design codes given in Table 4, and 64% of them have at least 1 vertical structural member that cannot satisfy the maximum axial stress limit of TBEC (2018). The damage photos given in subsequent parts of this study demonstrate that most of the examined buildings do not comply with the confinement provisions of the up-to-date seismic design codes. This observation is also supported by Aydogdu et al. (2023b) and others (i.e. Tapan et al. (2013) and Gurbuz et al. (2022)) stating that the columns of almost all pre-2000 building stock in Turkey have transverse reinforcement spacing between 200
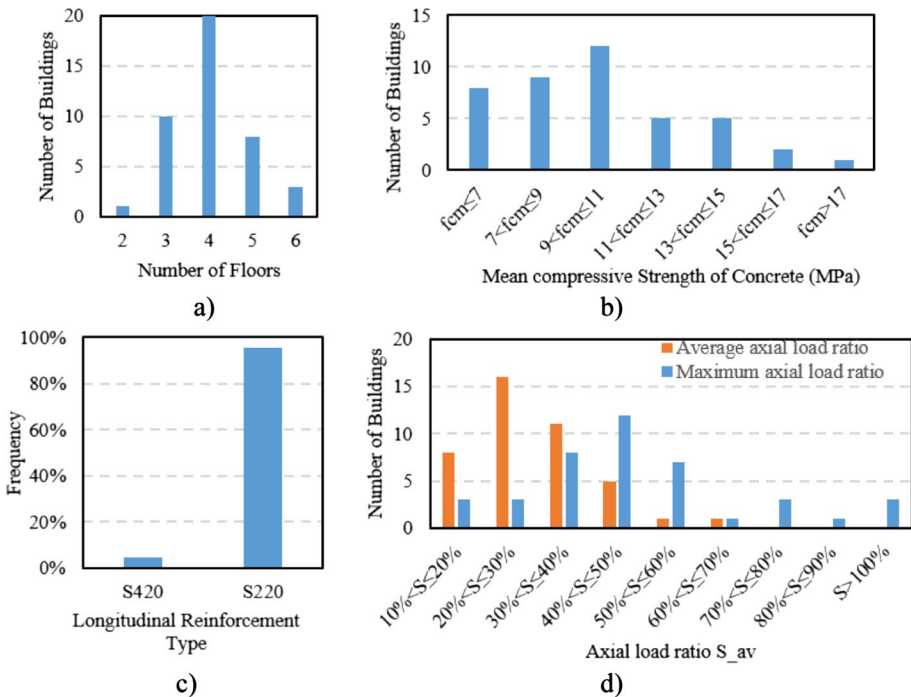

Fig. 5 Distribution of the structural parameters of the buildings: **a** number of floors, **b** equivalent cylindrical compressive strength of concrete (f_{cm}, from concrete hammer), **c** reinforcement steel class, where S420 is deformed and S220 is plain reinforcement bars, **d** average and maximum axial load ratio acting on vertical structural members

and 300 mm at the confinement zones. It can be inferred that these buildings, like many buildings constructed in the same period, are far from meeting the design and construction regulations of their era. This case may stem from the lack of control mechanism, seismic awareness and economic resources as narrated by Aydinoglu (2007), Ilki and Celep (2012), Makra et al. (2021), Gurbuz et al. (2022), Aydogdu et al. (2023b).

The most recent three seismic zoning maps in Turkey are given in Fig. 6a–c. According to the 1972 Seismic Zoning Map (Turkish Ministry of Public Works and Settlement), Bingöl and Afyon are in the second degree seismic zone, and Izmir is in the first degree seismic zone. By the 1996 Seismic Zoning Map (Turkish Ministry of Public Works and Settlement), the city center of Bingöl became a first degree seismic zone, and the rest of the cities stayed in the same seismic zone assigned by the previous map. In 2018, the zonation map concept was abandoned and a new coordinate-based earthquake hazard map was published (Turkish Ministry of Interior Affairs Disaster and Emergency Management Presidency, 2018). Change in the base shear coefficient for a representative building (5-story building with $V_{s30} = 300$ m/s soil condition) in Izmir, Afyon and Izmir districts according to various seismic design codes in Turkey is given in Fig. 6d. The base shear is the maximum shear force demand estimated, which is correlated with the effective seismic weight of the building, seismicity, soil parameters, the importance of the building and ductility of the system. The graph states that base shear demands for the representative buildings increased remarkably according to updated seismic design provisions in 1998, whereas the base shear demand slightly decreased for Afyon and Izmir in 2018. The evolution of the seismic design codes and seismic hazard maps in Turkey are summarized in the timeline given in Appendix 1 as well as the devastating earthquakes that happened in Turkey.

The building set consists of 35 reinforced concrete frame system buildings, while 7 of the buildings have dual reinforced concrete frame and wall structural systems. Dimensions of vertical structural members and structural system layouts of 8 representative buildings are given in Fig. 7. The rest of the layouts and structural information can be found in the SERU database (METU 2003). The compressive strength of the existing concrete is assigned based on the concrete hammer test results. A conversion equation of concrete hammer (Eq. 3), which is derived from the chart (Fig. 8a) provided by the manufacturer (Proceq 2002), is used to compute the equivalent of cubic ($15 \times 15 \times 15$ cm) compressive strength of concrete. The influence of the carbonation and the age of the concrete are also taken into consideration; a reduction factor depending on the age of the concrete, which is

Table 4 Minimum requirements in various Turkish Seismic Design Codes

	Seismic design code			
	1975	1998	2007	2018
Min. Longitudinal Reinforcement for Columns	1%	1%	1%	1%
Confinement Zone Max. Stirrup Spacing (cm)	10	10	10	10
135° Hook Ends	Yes	Yes	Yes	Yes
Min. Compressive Strength of the Concrete (MPa)	18	20	20	25
Compulsory Deformed Longitudinal Reinforcement	No	No	Yes	Yes
Max. $N_d/A_c f_{ck}$ allowed	0.6*	0.5	0.5	0.4
Shear Wall End Zones	Yes	Yes	Yes	Yes

*from TS500—Requirements for design and construction of reinforced concrete structures
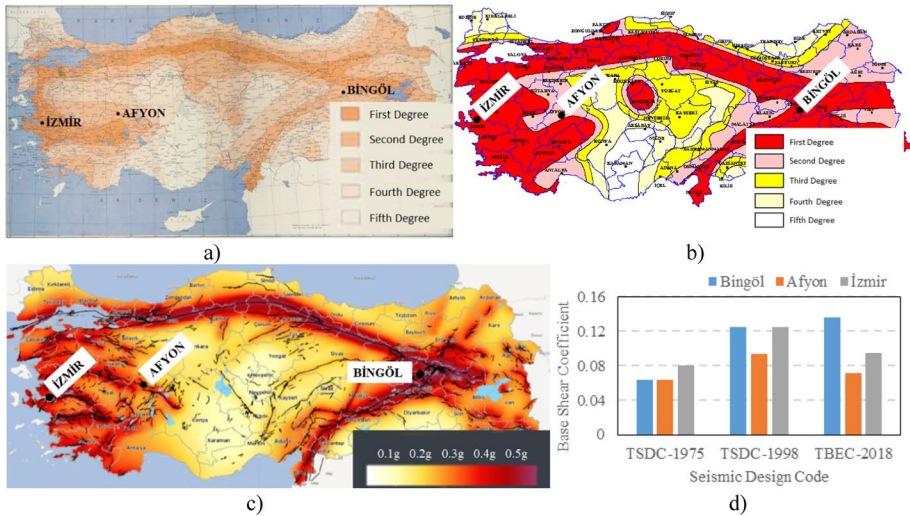
Fig. 6 **a** 1972 Turkish Seismic Zoning Map (Turkish Ministry of Public Works and Settlement), **b** 1996 Turkish Seismic Zoning Map (Turkish Ministry of Public Works and Settlement), **c** Earthquake Hazard Map of Turkey (Turkish Ministry of Interior Affairs Disaster and Emergency Management Presidency 2018), **d** Change in the base shear coefficient for a representative building in Izmir, Afyon and Izmir districts according to various seismic design codes in Turkey

also provided by the producer of the test hammer, is used (Fig. 8b). The cylindrical equivalent of the cubic compressive strength is determined through Eq. (4). To calculate the in-situ compressive strength of the concrete for the structures, Eq. (5) is used as suggested by Turkish Building Earthquake Code (2018).

$$f_{cc,i} = (0.0108 * n^2 + 0.9021 * n - 12.87) * A \tag{3}$$

$$f_{c,i} = \propto * f_{cc,i} \tag{4}$$

$$f_{cm} = max(0.85 * \sum_{i=1}^{z} \frac{f_{c,i}}{z}; \sum_{i=1}^{z} \frac{f_{c,i}}{z} - std.dev(f_{c,i})) \tag{5}$$

Note that n is the rebound number of the concrete test hammer, A is the age factor, $f_{cc,i}$ is the equivalent of cubic ($15 \times 15 \times 15$ cm) compressive strength of concrete, $\propto$ is the shape conversion factor to $15 \times 15 \times 15$ cm cubic strength to 10×10 cylindrical strength, $f_{c,i}$ is the cylindrical compressive strength of concrete, the z is the number of points that the non-destructive tests were performed, and f_{cm} is the estimated in-situ cylindrical compressive strength of the building.

The type of reinforcement bars for each building is reported in the SERU database (METU 2003). However, the information on the longitudinal reinforcement ratio for columns and shear walls, transverse reinforcement diameter and spacing, which are key parameters to perform PERA2019, are not specified in the database. To overcome this obstacle, reinforcement information and spacing values are determined from damage photos, when the reinforcements are visible. Otherwise, these parameters are selected based on assumptions made (Table 5) considering the common practice of construction along the
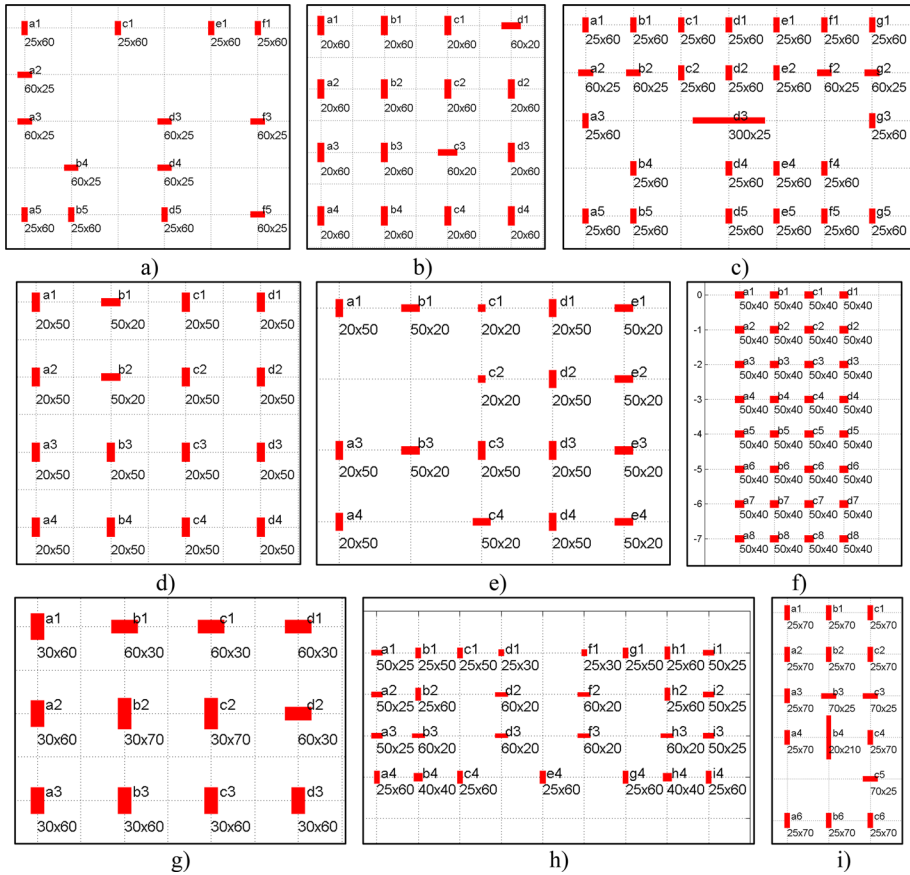
Fig. 7 Dimensions of vertical structural members and idealized layouts of representative buildings, **a** BNG-11-4-4, **b** BNG-6-4-3, **c** BNG-6-4-7, **d** AFY-Ç-06, **e** AFY-ÇO-05, **f** AFY-Y-01, **g** AFY-Ç-07, **h** AFY-ÇO-02, **i** Karşıyaka01 (units of column dimensions are cm). Building IDs are used as they are defined in the SERU database (METU 2003)

Fig. 8 **a** The conversion factor for the rebound number of the concrete hammer to equivalent cube strength, **b** age factor for concrete to take into account carbonation

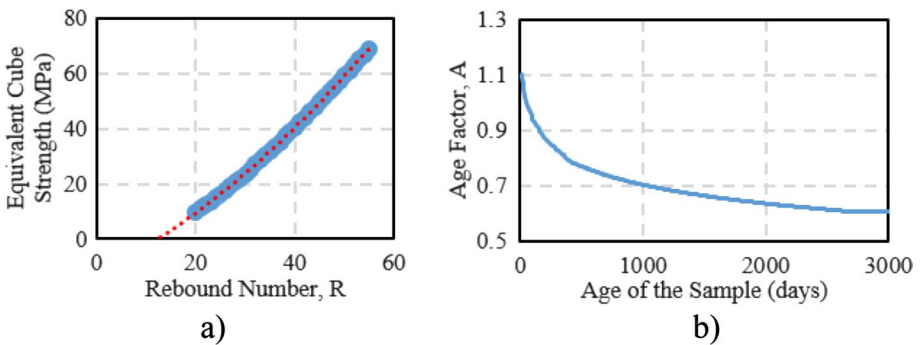**Table 5** The assumptions made in absence of data

Parameter	Requirements of TSDC-1975	Requirements of TSDC-1998	Year of construction	Assumption
Longitudinal Reinforcement Ratio	Min. 1.00%	Min. 1.00%	Before 1975	1.00%
			After 1975	0.75%
Transverse Reinforcement Spacing at Confinement Zone	Max. 10 cm	Max. 10 cm	Before 2000	25 cm
			After 2000	20 cm
Stirrup diameter	Min. 8 mm	Min. 8 mm		8 mm
Average Beam Cross-Section	Min. 20/30 cm	Min. 20/30 cm		25/60 cm

Table 6 General information on the considered earthquakes

Date	Epicenter	Depth (km)	M_W	Station (Code)	V_{s30} (m/s)	PGA (cm/s^2)	PGV (cm/s)	PGD (cm)	δ (°)
03.02.2002	Sultandağı— Afyon	22.1	6.5	Afyon (0301)	226	113	13	3	69
01.05.2003	Bingöl	10	6.3	Bingöl (1201)	529	501	37	16	82
30.10.2020	Aegean Sea— Izmir	14.9	6.6	Kuşadası (0905)	369	179	23	5	43

[*] The codes of the stations that recorded the PGA value are given in parentheses. The locations of these stations can be seen in Figs. 10, 13 and 16

range of construction years of the investigated buildings (Ilki and Celep 2012; Ilki et al. 2014; Yakut et al. 2021; Gurbuz et al. 2022; Aydogdu et al. 2023b) together with the minimum requirements of seismic design code valid at that time.

3.2 Earthquake events

General information on the earthquakes that the investigated buildings were subjected to is given in Table 6, and the acceleration-time histories of each earthquake are given in the following sections. The arias intensity is a significant indicator of the strength of a seismic event and demonstrates the time interval in which the energy of the ground motion is distributed. This parameter reflects the significant duration of an earthquake: the difference between the times when arias intensity is 5% and 95% is the significant duration according to Bommer and Martínez-Pereira (1999). Figure 9 demonstrates the arias intensities of the Afyon, Bingöl and Izmir earthquakes, and the significant durations of these earthquakes are 12.1 s, 4.6 s and 20.6 s respectively.

For the buildings in Bingöl and Izmir, the orientation of the buildings was recorded on the plans. Therefore, the horizontal components of the strong ground motions were processed and adapted to be applied along their main orthogonal directions to accurately represent the seismic actions that these buildings were subjected to. The direction of the plan and response in both directions can be extremely critical during an earthquake for irregular structures, the effect of which was studied in detail by Cimellaro et al. (2014). On the other hand, the orientations of buildings in the plans were not noted for the buildings examined in Afyon. Therefore, in absence of information on the plan orientation of the buildings, the

geometric mean spectrum of the strong ground motion couple is assigned as seismic demand in both X and Y directions of the buildings in Afyon. Since the buildings in Izmir are very close to strong ground motion recorders in Karşıyaka and Bostanlı districts, acceleration records of these stations were directly used in the analyses. The spectral acceleration value at the first mode period of the building is defined as the seismic demand of the building.

In the case of the Afyon and Bingol earthquakes, there was only one strong ground motion record for each. Therefore, ground motion prediction equations (GMPE) were used to reduce the uncertainties for the investigation of buildings in Afyon and Bingol. For this purpose, Abrahamson and Silva (2008) ground motion prediction equations (GMPE) were used in order to obtain the acceleration spectrum that the buildings were subjected to for the location of each building. The GMPE was developed to estimate the acceleration spectrum and logarithmic standard deviation values for any specific earthquake. The model is applicable to magnitudes between 5 and 8.5 and distances between 0 and 200, according to developers of the GMPE. In order to reduce the uncertainties of the ground motions for each seismic event, residuals must be calculated for every location of ground motion recorders in that event to visualize the spatial distribution of the residuals. However, there is a single record for Afyon and Bingol events. Therefore, the spatial distribution of residuals couldn't be produced. To overcome this problem, Bal and Smyrou (2016) proposed an assumption of identical intra-event variability and equal residuals for two locations for the same event. The same approach was used in this study. Several parameters are required for computing the GMPE functions. M_w is the moment magnitude of the event, R_{rup} is the closest distance to the surface rupture, R_x is the horizontal distance to the rupture, W is the rupture width of the fault, R_{jb} is the Joyner-Boore distance, δ is the dip angle, V_{s30} is the average shear-wave velocity of the top 30 m of the soil, Z_{tor} is the depth to the top of rupture and calculated in accordance with the empirical equation introduced by Mai et al. (2005), Z_{HYP} is the hypocentral depth, $Z_{1.0}$ is the depth to a shear-wave velocity of 1.0 km/s at the site. The authors of the used GMPE also recommend scaling for hanging wall sites, the effect of which is evaluated by Beyen (2018). After implementation of the GMPE, median acceleration spectrum (μ) and logarithmic standard deviation of spectral acceleration estimation (σ) parameters are yielded as outputs. TBEC (2018) proposes a scaling procedure between 0.2 and 1.5 times the fundamental period of the structure. Scaling dependent to the first mode period of a structure will yield different scaling factors for two buildings in the same location. However, a location can have only one residual value for a seismic event. Thus, the spectral match is performed over the range of 0.3 s and 2.0 s

Fig. 9 Arias intensity curves computed for N-S records of all investigated earthquakes
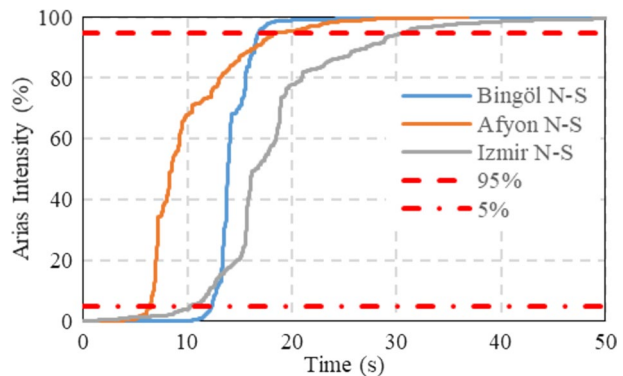
periods, which covers %99 of the periods of approximately 25,000 investigated reinforced concrete buildings according to Aydogdu et al. (2023b).

3.2.1 2002 Afyon earthquake

According to the Disaster and Emergency Management Presidency, the city center and districts of Afyon province were shaken on 3 February 2002 by a $M_w = 6.5$ earthquake with a 22.1 km focal depth which was also felt strongly in surrounding cities (Url-1 2020). The acceleration records taken from the Afyon city center are given in Fig. 10. The event occurred on a normal fault zone. The closest ground motion record was taken in the city center of Afyon. The investigated buildings for this earthquake were located in 6 different spots: Afyon city center, Çay, Çobanlar, Sultandağı, Bolvadin and Yeşilçiftlik neighborhoods (Fig. 11).

According to the geology map, the buildings investigated within the scope of this study are on similar geological formation. Akşehir and Eber Lakes and Aksu Stream are located circumference of the field of study, where the soil consists of alluvial sediments. These locations are also represented with similar V_{s30} values according to the global V_{s30} map (Url-2 2022). Thus, the V_{s30} value (226 m/s) of the ground motion recorder in Afyon, which is provided by TADAS database (AFAD 2020), is assigned to all other locations. The parameters needed to perform the computation for Abrahamson and Silva (2008) equations to obtain acceleration spectra for each district are given in Table 7. W, Z_{tor} and $Z_{1.0}$ values are 12 km, 14.9 km and 625 m for all locations, respectively.

Acceleration spectra of east–west and north–south components of the Afyon record and GMPE results are given in Fig. 12a. Here, AS indicates results of GMPE defined by Abrahamson and Silva (2008). Spectral matching is performed to equalize the areas under the period range between 0.3 s and 2.0 s, which is the expected period range of the structures examined in this paper. For the east–west component of the earthquake, a spectral match is reached with the $\mu + 0.18\sigma$ spectrum of the GMPE, while for the north–south component, the overlap is with the $\mu + 0.13\sigma$ spectrum. As aforementioned, the geometric mean spectra of GMPE results are assigned as seismic demand in both X and Y directions of the buildings in Afyon in absence of plan orientations of these buildings. The geometric mean spectrum of the GMPE result couple for these values is given in Fig. 12b. The logarithmic standard deviation difference between the observed and predicted spectral value is determined as the residual (ε). Since there is no other available strong ground motion record for this event, the calculated residual for the location of the strong ground motion recorder is
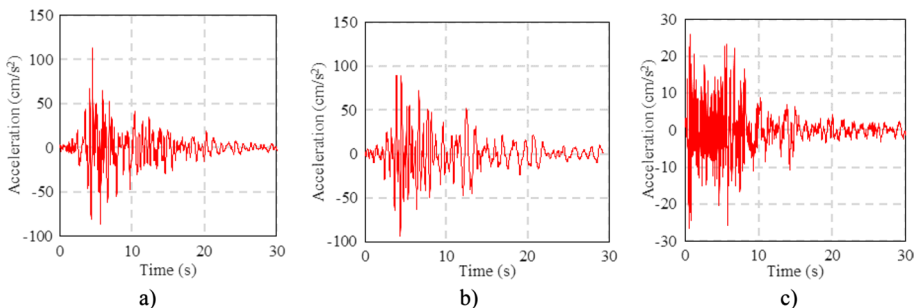

Fig. 10 Acceleration-time histories for the Afyon earthquake: **a** N-S record, **b** E-W record, **c** Vertical record (TADAS database, AFAD 2020). V_{s30} parameter of the site, of which the recorder is located, is 226 m/s
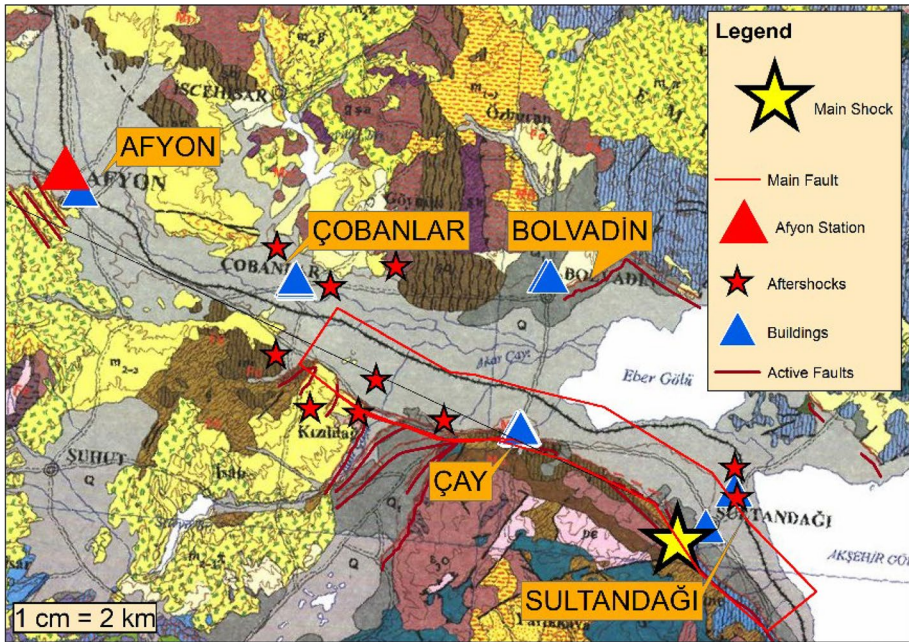
Fig. 11 Geology map of Afyon province (taken from the General Directorate of Mineral Exploration and Research). The main event, aftershocks, fault zone and buildings are shown on the map

appointed for every location for this seismic event, and the demand spectra for all districts are computed accordingly (Fig. 12c).

3.2.2 2003 Bingöl earthquake

On 1 May 2003, a $M_w = 6.4$ earthquake struck Bingöl province which occurred on a strike-slip fault (Url-3 2020). The earthquake was felt strongly in surrounding towns. The epicenter of the event is about 14 km northwest of Bingöl. The strong ground motion records obtained from the city center are the only available data for this earthquake (Fig. 13). The main fault, and locations of examined buildings, aftershocks and the seismic station are demonstrated on the geology map of the province (Fig. 14). The spatial distribution of the aftershocks with M > 4 is in the north-northwest direction for Bingöl city. Also, having a 2.23 km R_{jb} value according to the Disaster and Emergency Management Presidency of

Table 7 The parameters needed to calculate the GMPE

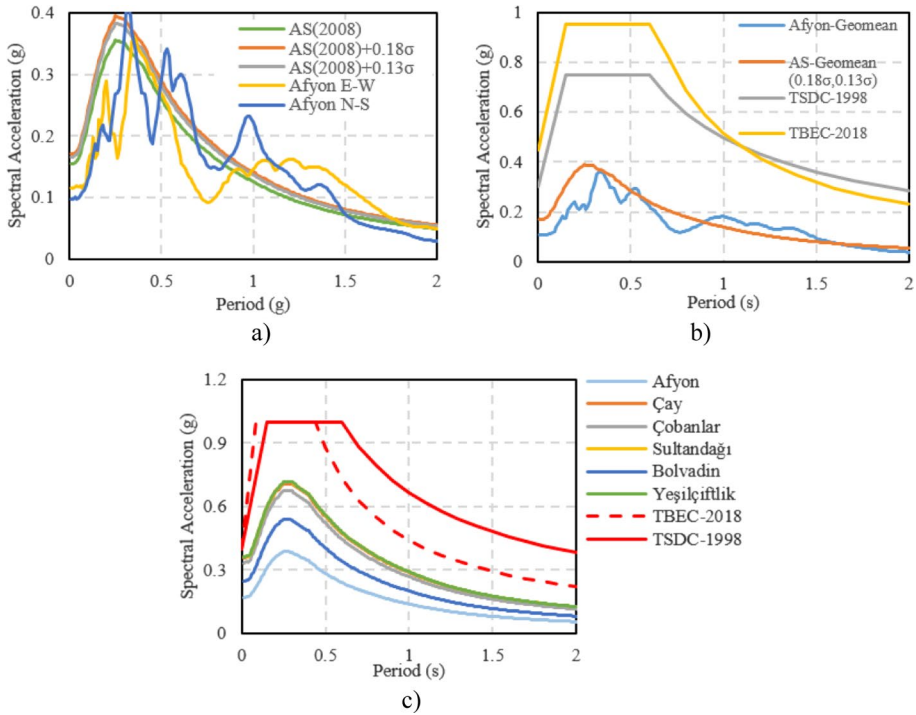| Location	R_{rup} (km)	R_{jb} (km)	R_x (km)
Afyon (Station)	40.8	31.4	4.8
Sultandağı	14.9	0.0	3.1
Çay	14.9	0.0	1.2
Bolvadin	28.3	10.8	15.1
Çobanlar	17.1	8.5	5.7
Yeşilçiftlik	15.5	4.1	7.4

Fig. 12 **a** Acceleration spectra of east–west and north–south components of Afyon record with matched spectra of GMPE, **b** geometric mean spectrum of Afyon record and the design spectrum of the central district of the city according to TSDC (1998) and TBEC (2018), **c** GMPE results for 6 different locations and the design spectrum of Çay district according to TSDC (1998) and TBEC (2018)

Turkey, it is accepted that the ruptured segment of the fault extends into the Bingöl city center. The peak spectral acceleration of this earthquake is 2.4 g at 0.16 s period for the N-S component of the record. Such a great seismic demand is expected to create widespread destruction in the city. However, as aforementioned, the significant duration of the earthquake is relatively short compared to the other earthquakes.

According to the local soil parameters of the seismic station, the recorder is established on relatively hard soil ($V_{s30} = 529$ m/s). However, the rest of the city is estimated to be on relatively loose soil, based on the Bingöl Earthquake Evaluation Report of the General Directorate of Mineral Exploration and Research (2003) which states that the soil characteristics change from rock formations to fine-grained sediments when going from east to west or towards the plain. Likewise, the global V_{s30} map of USGS (Url-2 2022) suggests 256 m/s shear wave velocity for the plain of Bingöl. As shown below, the locations of the investigated buildings in Bingöl are grouped into four zones, based on the ground conditions. Correspondingly, the GMPE calculations are made to determine the acceleration spectra for these four zones:

- First Zone: Stiff soil and close to the strong ground motion recorder (3 buildings).
- Second Zone: Loose soil in the eastern part of the city (3 buildings).
- Third Zone: Loose soil in the western part of the city (15 buildings).

Fig. 13 Acceleration-time histories for the Bingöl earthquake: **a** N-S record, **b** E-W record, **c** Vertical record (TADAS database, AFAD 2020). V_{s30} parameter of the site, of which the recorder is located, is 529 m/s
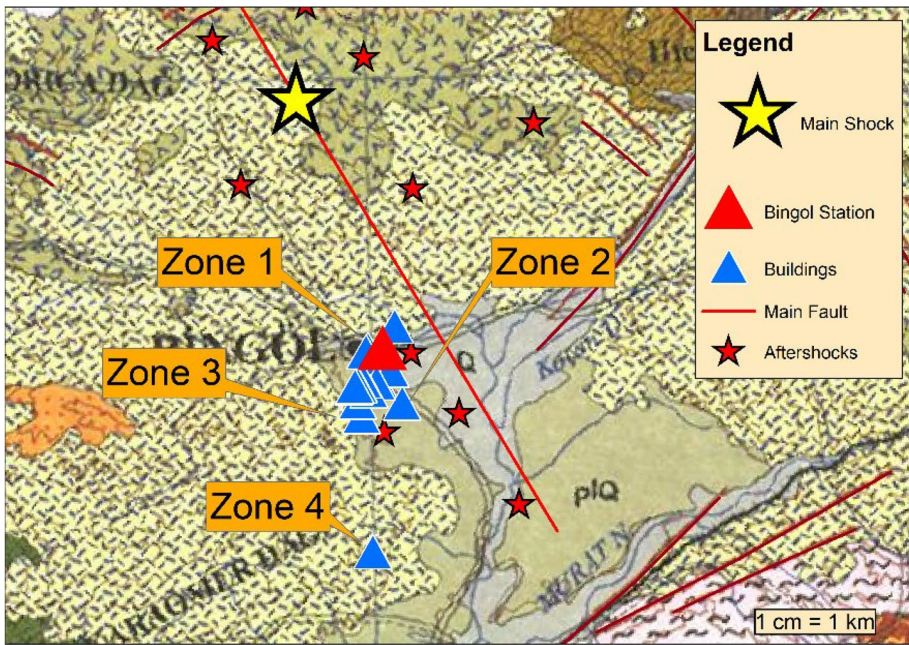
Fig. 14 Geology map of Bingöl province (taken from the General Directorate of Mineral Exploration and Research). The main event, aftershocks, fault line and the buildings are shown on the map

– Fourth Zone: Loose soil 9 km southwest of the city (1 building).

The parameters needed for the calculation of GMPEs for these locations are given in Table 8. W and Ztor values are 8.7 km and 4.8 km for all locations, respectively.

Acceleration spectra determined by the GMPE approach presented above and computed based on east–west and north–south components of the Bingöl record are given in Fig. 15a. Acceleration spectra of the record and GMPE results between 0.3 s and 2.0 s are matched.

For the east–west component of the earthquake, a spectral match is reached with the μ-0.18σ spectrum of the GMPE, while for the north–south component, the overlap is obtained with the μ+0.55σ spectrum. The matched spectra with north–south and east–west components for each zone are given in Fig. 15b and c, respectively. Similar to Afyon Earthquake; the calculated residual of the acceleration record is appointed to every other location.

3.2.3 2020 Izmir earthquake

An earthquake with $M_w=6.6$ occurred in the Aegean Sea on 30 October 2020. Even though the distance is nearly 80 km far from the epicenter, which is northeast of Samos Island, Izmir city center was affected by the earthquake seriously. The acceleration records taken from the Izmir city center (Karşıyaka district) are given in Fig. 16. The main shock occurred on a normal fault (TADAS database, AFAD 2020). Two buildings that experienced this earthquake are evaluated within the scope of this study. The buildings are located in the vicinity of the recorders in Karşıyaka and Bayraklı districts (Fig. 17a). Thus, acceleration spectra of corresponding records are assigned as demand spectrum directly. The record couples are rotated based on the orientation of the building (Fig. 17b).

4 Results and discussion

4.1 Structural damages

In the literature, there are post-earthquake damage assessment methods at different levels of detail. Since the number of damage photos of the examined buildings is limited, the rapid damage inspection approach, which is the quickest among the other methods, introduced by damage assessment trainings of the Turkish Ministry of Environment, Urbanization and Climate Change is used to assign the damage levels to the examined buildings. The general flowchart of the damage assessment procedure is given in Fig. 18. Damage information of the buildings with an insufficient number of photos is taken directly from the SERU database. The damage classification of reinforced concrete members is made based on the damage limits given in Table 9 (Ilki et al. 2020, 2021b; Akkar et al. 2021).

A lightly damaged building is given in Fig. 19. The building contains a column with a Type A shear crack and is identified as slightly damaged since it does not have any higher damage type elements. A building that experienced Afyon Earthquake (2002), which was under construction during the earthquake, is shown in Fig. 20a. The building contains a Type B flexural crack (Fig. 20b). However, owing to the Type D damages illustrated in Fig. 20c, the building is categorized as heavily damaged.

Table 8 The parameters needed to calculate the GMPE	Zone	R_{rup} (km)	R_{jb} (km)	R_x (km)	$Z_{1.0}$ (m)	V_{s30} (m/s)
	1 (Recorder)	5.8	2.2	2.2	171	529
	2	5.4	2.5	2.5	545	250
	3	6.2	4.0	4.0	545	250
	4	9.8	8.6	7.0	545	250
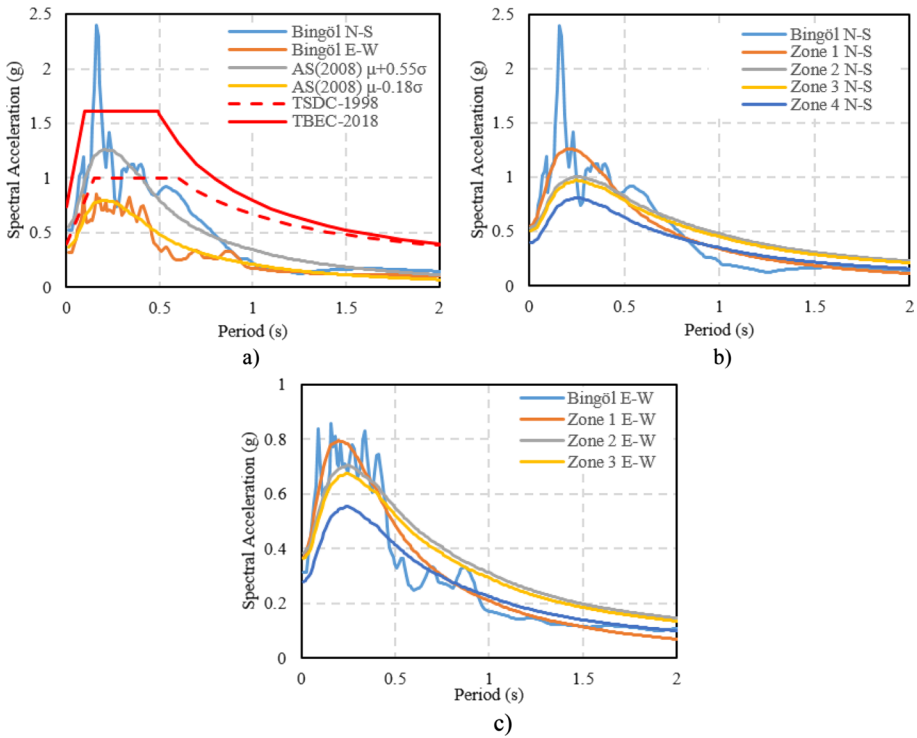
Fig. 15 **a** Acceleration spectra of east–west and north–south components of the record with matched spectra of GMPE and the design spectrum of the site accordis + 0.55 ε, **c** GMPE results for east–west direction for each location with μ − 0.18 ε
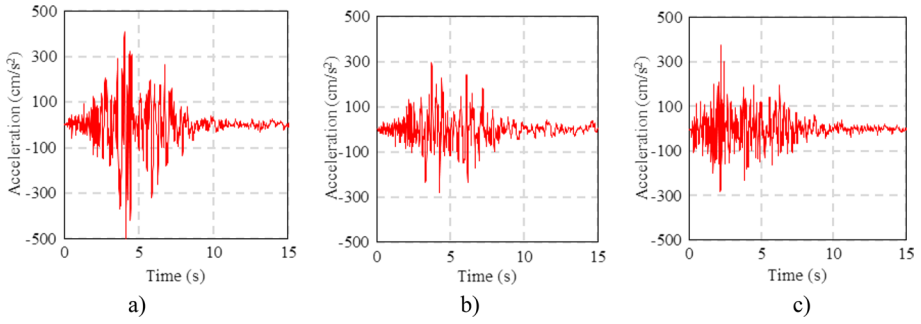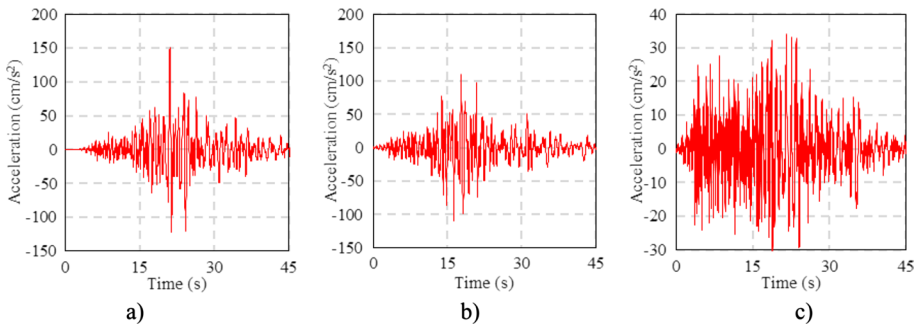

Fig. 16 Acceleration-time histories for the Izmir earthquake: **a** N-S record, **b** E-W record, **c** Vertical record (TADAS database, AFAD 2020). V_{s30} parameter of the site, of which the recorder is located, is 131 m/s

At least two columns of the building shown in Fig. 21a experienced Type C damage. In Fig. 21b, c, two examples of spalling of concrete cover are given. The building also has elements with Type D damage. Thus, the damage state of the BNG-6–4-2 building is decided as heavy damage. Figure 22a shows another building that experienced Bingöl Earthquake (2003) and was subjected to heavy damage. Vertical reinforced concrete members of the
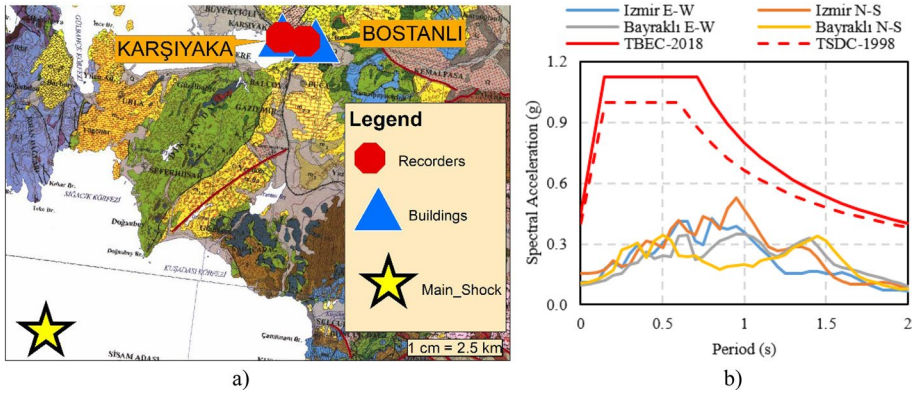
Fig. 17 **a** Geology map (taken from the General Directorate of Mineral Exploration and Research) and the locations of the buildings and strong ground motion stations (records), **b** Acceleration spectra of the records and the design spectrum of the site according to TSDC (1998) and TBEC (2018)

building exhibited Type D shear crack, reinforcement buckling, crushing of concrete core and rupture of transverse reinforcement (Fig. 22b, c).

The individual damage states determined for all evaluated buildings through the rapid damage assessment procedure explained above are given in Appendix 2. The final damage distribution for each seismic event is given in Table 10. It should be noted that the only considered earthquake that had a significant aftershock among others is the Afyon earthquake. The mainshock was followed by a $M_w = 5.8$ aftershock, the recorded PGA values of which were around 0.04~0.05 g. Since the PGA values of the aftershock are not significant enough, it is assumed that damage states of buildings in Afyon occurred after the main shock.
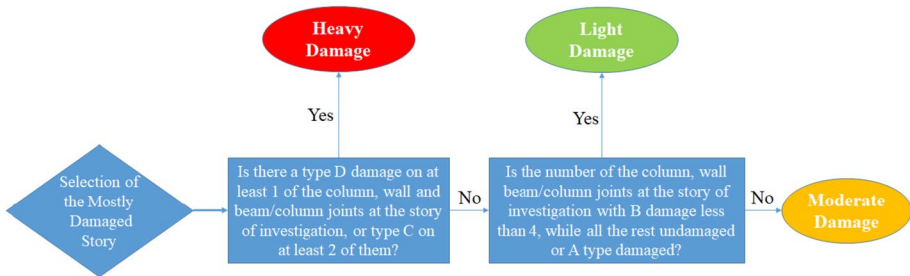
Fig. 18 Decision tree algorithm for rapid damage assessment

Table 9 Element damage type classification

Damage type	Crack width	Compression damage
0	–	–
A	$w \leq 0.5$ mm	–
B	$0.5 < w \leq 3.0$ mm	Crushing of Concrete Cover
C	–	Spalling of Concrete Cover
D	–	Reinforcement Buckling—Crushing of Concrete Core

Fig. 19 **a** The BNG-5–5-1 building (lightly damaged), **b** Type A shear crack (METU 2003)

4.2 Results obtained by performance based rapid seismic safety assessment methodology

The SSR values of investigated 42 buildings are determined through the implementation of the PERA2019 procedure and are compared with the actual damage states of the buildings that have been exposed to one of the 2002 Afyon, 2003 Bingöl or 2020 Izmir earthquakes to evaluate the reliability and safety margin of proposed performance based rapid seismic assessment method. As shown above, the amplitude of acceleration spectra computed for ground motion records of the 2002 Afyon and 2020 Izmir earthquakes is slightly less than the design spectra of the seismic design codes, while the acceleration spectrum of 2003 Bingöl earthquake is closer to the design spectrum and even higher in the short-period range compared to other seismic events. Obviously, there should have been no seismic-induced collapse or heavy damage if the examined buildings have been constructed in accordance with the seismic design codes of their eras.

Comprehensive information on the global damage levels, SSR values determined by the application of PERA2019, and structural properties such as the first period of vibration, base shear demand, axial stress on vertical elements, reinforcement details, material properties, and plan dimensions for each building are given in Appendix 2. The trends between the observed damage levels and various structural parameters are illustrated in Fig. 23. The findings of the study show that seismic-induced damages for buildings with the same number
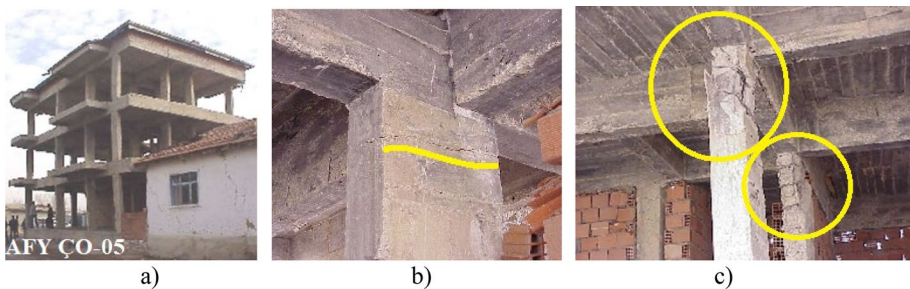
Fig. 20 **a** The AFY-ÇO-05 building (heavily damaged), **b** Type B flexural crack, **c** Type D flexural and shear damages (METU 2003)
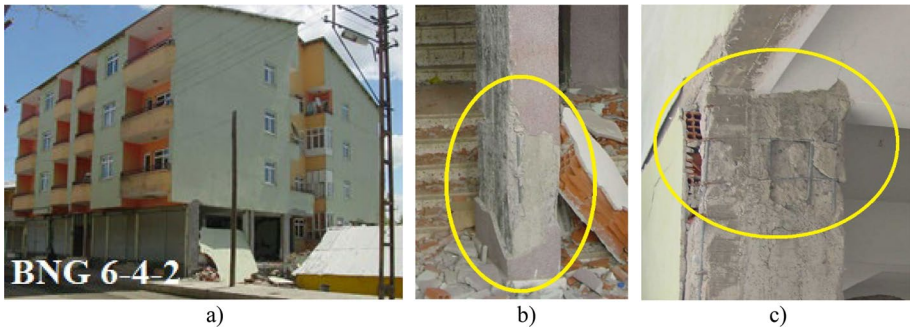
Fig. 21 a The BNG-6-4-2 building (heavily damaged), **b** Type C damage: Spalling of Concrete Cover, **c** Type C damage: Spalling of Concrete Cover (METU 2003)

Fig. 22 a The BNG-6-3-1 building (heavily damaged), **b** Type D shear crack, reinforcement buckling, crushing of concrete core and rupture of transverse reinforcement, **c** Type D flexural damage with crushing of concrete core and buckling of longitudinal bars (METU 2003)

Table 10 Damage distribution of the buildings for considered seismic events

		Damage type				
		Collapse	Heavy	Moderate	Light	None
Event	Afyon	1	10	3	4	0
	Bingöl	1	8	5	5	3
	Izmir	0	0	0	0	2
	Total	2	18	8	9	5

of stories can be at different levels. Hence, it would not be realistic to perform a building scale seismic evaluation based only on their number of stories. The compressive strength of the existing concrete is a critical parameter for the seismic performance of RC buildings. The relationship between observed damage levels and the compressive strength of the existing concrete does not exhibit a good trend. The building in which the highest compressive strength of the existing concrete is measured has collapsed, and the building with the lowest compressive strength of the existing concrete has not experienced any seismic damage.

Also, the comparison of the average axial load on columns at the critical story resulting from gravity loads and the observed damage states of the buildings shows a large scatter. Thus, estimating the seismic safety of individual buildings using simplified procedures without considering all crucial structural parameters may lead to grave misclassifications.

Figure 24a demonstrates the harmony of the observed damage levels with SSR values and risk classes of the buildings computed through the implementation of the PERA2019 methodology. On contrary to the inadequate consistency of individual structural parameters investigated above compared to structural damages, the SSR values obtained for the examined buildings exhibit good conformity with observed damages and tend to decrease as the damage state increases. Figure 24b illustrates the risk class ratios of the buildings for each damage state group. Seismic risk classes of the buildings also show a promising consistency with the observed damages too.

The proposed methodology satisfactorily labels all collapsed buildings as E class, which corresponds to a very high seismic risk. The buildings severely damaged are also classified as either E or D class. Moreover, the SSR region above 40% does not contain any heavily damaged or collapsed buildings, which is a good safety indicator because a buffer zone of SSR values between 40 and 50% does not include any heavily damaged or collapsed buildings, while this range of SSR is still in D Class. Distinguishing the buildings with good seismic performance from the ones with poor seismic performance is another critical aspect of seismic assessment methods. The results of this study show that PERA2019 is able to determine almost 80% of the buildings without seismic damage or lightly damaged ones as C, B or A class, while none of them is categorized as E class or very high risk.

Table 11 yields the comparison of risk classes based on the SSR values and observed structural damage levels. The matrix given below illustrates the safe and unsafe classifications. According to numerical values given in Table 11, as expected, the average SSR values of the buildings in each observed damage group also decrease as the damage state increases. This study demonstrates that the present risk classification method is rational and contains a good safety margin. On the other hand, conducting site investigations after future earthquakes and adding more building data will increase the accuracy of this case study. The presented methodology is a rapid and approximate second-stage performance-based procedure, and exact results are not expected at this level of assessment. The target of this methodology is rapid and cost-effective prioritization of existing buildings with
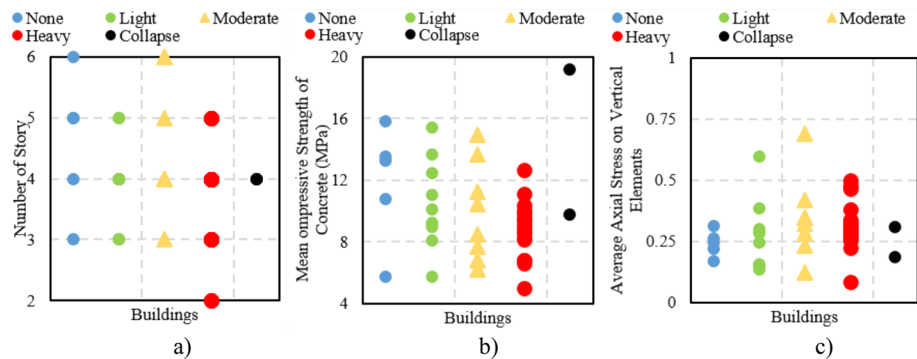

Fig. 23 The trends between the observed damage levels and various important structural parameters of the buildings: **a** Number of stories, **b** compressive strength of the existing concrete, **c** average axial stress on vertical members. The horizontal axis illustrates different damage state groups
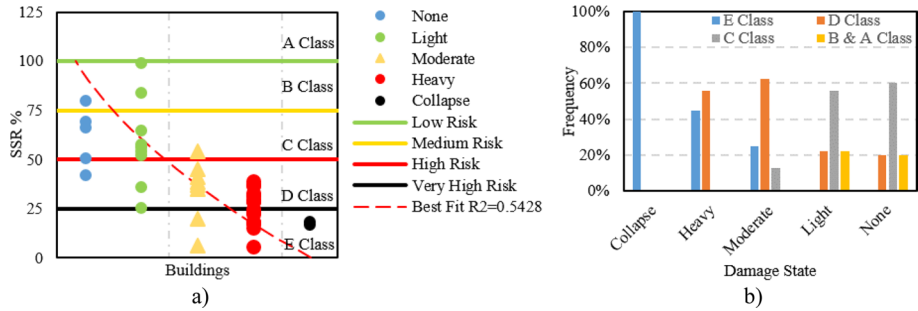
Fig. 24 **a** Distribution of SSR values of the investigated buildings computed through PERA2019 for each damage level groups, **b** histogram of risk class distributions for each damage level groups

respect to their seismic risks to allocate limited sources/budget to further detailed analysis of those buildings which are prone to the highest risks. And such scaling down process of the huge problem is very important for cities like Istanbul with hundreds of thousands of substandard buildings. It should be further noted that the methodology has been validated through means of other methods, such as numerical analyses as aforementioned.

5 Conclusions

This study was conducted as the first step of the validation efforts of the proposed seismic risk classification/prioritization procedure. Within the scope of this study, SSR values of 42 buildings that experienced real seismic actions (2020 Afyon, 2003 Bingöl and 2020 Izmir earthquakes) were evaluated through PERA2019 rapid seismic performance assessment methodology in a blind manner and then the estimated SSRs of the buildings were compared to the observed seismic-induced damages to determine the reliability and safety margin of the proposed risk classification approach. It should be noted that the spectral accelerations calculated for the three strong ground motions presented in this study are quite close to the spectral design accelerations for Afyon, Bingöl and Izmir for a wide range of frequencies.

The results of this study demonstrated that the SSR values increase as the damages of the building decrease. The proposed risk classification approach succeeded to label all of the collapsed buildings in E Class (very high seismic risk). Moreover, all of the buildings subjected to heavy damage were classified as E or D Class, which correspond to very high and high seismic risk respectively. Risk classes of 96% of the moderately, heavily damaged or collapsed buildings that cannot be inhabited after the earthquake were determined as high or very high risk. Also, all of the severely damaged or collapsed buildings had an SSR value of less than 40%, which is a good safety indicator because a buffer zone of SSR values between 40 and 50% does not include any heavily damaged or collapsed buildings, while this range of SSR is still in D Class. This output demonstrates that the present risk classification method contains a good safety margin. As important as specifying the buildings with poor seismic performance, identifying the buildings with good seismic performance from the seismically deficient ones is another crucial task for risk mitigation efforts. Therefore, to evaluate the reliability of a seismic risk classification method, categorizing the buildings with adequate seismic performance in low risk class has grave importance, as well as determining the buildings with poor seismic performance as high risk. A method cannot be stated as successful as long

Table 11 Comparison of risk classes (determined based on SSR values) and observed global damage levels (red-colored cells are unsafe classification regions)

		Observed Global Damage				
		Collapse	Heavy	Moderate	Light	None
PERA2019 Risk Class	E (Very High Risk)	2	8	2	0	0
	D (High Risk)	0	10	5	2	1
	C (Medium Risk)	0	0	1	5	3
	B-A (Low Risk)	0	0	0	2	1
	SSR Range %	17–18	6–39	6–54	25–99	42–80
	Average SSR %	17.7	25.9	34.6	58.7	61.6
	Std. Dev. SSR %	0.6	8.5	14.0	21.1	13.6

as the method classifies the buildings with good seismic performance as high risk buildings. Based on the findings of this study, PERA2019 is able to classify almost 80% of the buildings without seismic damage or light damage as C, B or A class, while none of them is classified as high (D class) or very high risk (E class). The trends between the observed damage levels and structural parameters showed that individual structural parameters do not have sufficient conformity with the damage states of the buildings, even though structural parameters affect global seismic performance. Further site investigations are to be conducted after future earthquakes as well as additional numerical analyses to support current findings with further evidence in terms of the reliability of the presented approach.

Appendix 1: The evolution of the seismic design codes and seismic hazard maps in Turkey and the devastating earthquakes that happened in Turkey.
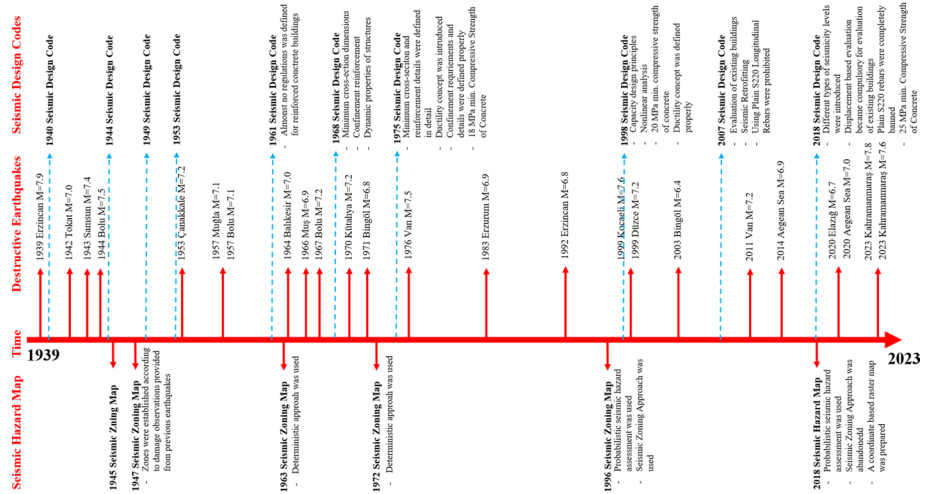
Appendix 2: Structural parameters, PERA2019 results and damage information of the buildings

Building Code	SSR-Y	SSR-X	SSR	Global Observed Earthquake Damage	Max. axial stress	Aver-age	Period in Y Direction (s)	Period in X Direction (s)	Base Shear in Y Direction (kN)	Base Shear in X Direction (kN)	f_c (MPa)	f_s (MPa)	Stirrup Spacing (cm)	Number of Columns	Number of Risky Columns	Spectral Acceleration Demand (g)	Spectral Acceleration Demand_y (g)	Number of Floors	Total Floor Area (m2)	Year of construction	Total area of vertical structural elements (cm2)	Longitudinal Reinforcement Ratio (%)	Type of Use
BNG-10-4-9	69.3	94.0	69.3	None	53%	25%	0.46	0.45	21,298	14,478	13.5	420	20	33	3	0.58	0.86	5	2476	2002	123,700	1.0%	Residential
BNG-3-4-4	42.0	72.0	42.0	None	38%	22%	0.48	0.58	14,296	9656	10.8	220	25	53	15	0.51	0.75	4	1900	1980	91,700	1.0%	Residential
BNG-6-3-11	50.4	50.4	50.4	None	38%	31%	0.53	0.53	4625	4599	5.8	220	25	26	26	0.65	0.66	3	705	1980	39,000	1.0%	Residential
Karsiyaka01	129.0	80.0	80.0	None	34%	26%	0.95	1.10	2602	2290	13.2	220	10	16	3	0.23	0.26	6	1014	1998	30,450	1.1%	Residential
Izmir01	70.5	66.4	66.4	None	28%	17%	0.78	0.75	1265	1297	15.8	220	20	13	4	0.28	0.27	5	462	1985	17,250	0.5%	Residential
BNG-10-4-7	48.6	39.7	39.7	Light	59%	24%	0.55	0.75	25,578	13,411	9.3	220	25	69	65	0.41	0.77	4	3311	1988	164,225	1.0%	Residential
BNG-10-5-11	114.3	57.6	57.6	Light	32%	13%	0.49	0.61	3132	2994	13.7	220	25	13	13	0.65	0.68	5	460	1988	26,525	1.0%	Residential

Building Code	SSR-Y X	YSSR-SSR	Global SSR	Observed Earthquake Damage	Max. axial stress	Average axial stress	Period in Y Direction (s)	Period in X Direction (s)	Base Shear in Y Direction (kN)	Base Shear in X Direction (kN)	f_c (MPa)	f_s (MPa)	Stirrup Spacing (cm)	Number of Columns	Number of Risky Columns	Spectral Acceleration Demand_x (g)	Spectral Acceleration Demand_y (g)	Number of Floors	Total Floor Area (m2)	Year of construction	Total area of vertical elements (cm2)	Longitudinal Reinforcement Ratio (%)	Type of Use
BNG-3-4-1	79.0	36.0	36.0	Light	40%	28%	0.52	0.51	10,122	14,817	8.1	220	25	50	50	0.77	0.52	4	1930	1998	85,000	1.0%	Residential
BNG-5-5-1	25.2	56.7	25.2	Light	61%	38%	1.02	0.85	8725	6850	9.0	220	25	32	32	0.35	0.44	5	1974	1985	57,875	1.0%	Residential
BNG-6-3-4	56.0	116.0	56.0	Light	20%	15%	0.49	0.40	2396	2724	12.5	220	20	12	6	0.83	0.73	3	329	2003	18,000	1.0%	Residential
AFY-B-02	170.0	99.0	99.0	Light	47%	16%	0.47	0.58	5763	4761	15.4	220	25	26	10	0.35	0.43	3	1042	1976	61,650	1.0%	Public
AFY-Ç-11	111.6	83.7	83.7	Light	20%	15%	1.14	1.22	3278	2981	11.0	220	20	31	31	0.22	0.24	4	1341	2002	78,463	1.0%	Residential
AFY-ÇO-04	84.6	64.8	64.8	Light	51%	30%	0.71	0.77	3400	3188	5.7	220	25	22	12	0.35	0.38	4	903	1994	52,800	1.0%	Residential
AFY-M-02	66.0	52.0	52.0	Light	80%	60%	0.96	1.21	4775	3507	10.1	220	25	40	32	0.11	0.14	4	2551	1970	57,600	1.0%	Public
BNG-10-3-3	54.0	38.7	38.7	Moderate	37%	23%	0.60	0.63	7786	7779	7.7	220	30	24	24	0.65	0.65	3	918	1975	67,200	0.7%	Public
BNG-10-4-4	32.8	19.7	19.7	Moderate	59%	42%	0.76	0.92	23,704	13,659	8.5	220	25	57	57	0.33	0.57	6	4159	1998	117,850	1.0%	Residential
BNG-10-4-6	48.1	34.3	34.3	Moderate	47%	16%	0.64	0.49	14,315	26,154	14.9	220	25	61	29	0.84	0.46	4	2408	1976	137,822	1.0%	Residential

Building Code	SSR-X	SSR-Y	SSR-Global	Global Observed Max. Earthquake Damage	Observed axial stress	Average axial stress	Period in Y Direction (s)	Period in X Direction (s)	Base Shear in Y Direction (kN)	Base Shear in X Direction (kN)	f_c (MPa)	f_s (MPa)	Stirrup Spacing (cm)	Number of Columns	Number of Risky Columns	Spectral Acceleration Demand_x (g)	Spectral Acceleration Demand_y (g)	Number of Floors	Total Floor Area (m2)	Year of construction	Total area of vertical elements (cm2)	Longitudinal Reinforcement Ratio (%)	Type of Use
BNG-10–5-1	38.7	27.0	27.0	Moderate	109%	45%	1.05	1.64	16,130	10,045	10.5	220	30	41	41	0.24	0.39	6	3210	1990	108,925	1.0%	Residential
BNG-10–5-2	23.4	6.3	6.3	Moderate	109%	69%	1.46	1.95	6826	6903	6.2	220	25	32	32	0.23	0.22	5	3059	1990	75,300	1.0%	Residential
AFY-B-01	53.9	83.1	53.9	Moderate	95%	32%	0.99	0.91	4884	5296	11.2	220	40	37	24	0.22	0.20	4	1853	1974	78,900	0.7%	Public
AFY-Ç-05	64.0	45.0	45.0	Moderate	43%	28%	0.65	0.79	2704	2230	13.7	220	25	16	16	0.36	0.44	4	615	1985	16,000	0.7%	Residential
AFY-Ç-12	66.6	36.9	36.9	Moderate	54%	35%	0.68	1.19	2705	1503	6.8	220	25	20	20	0.23	0.42	4	649	1985	27,500	1.0%	Residential
BNG-10-3-10	17.7	18.4	17.7	Heavy	49%	38%	0.53	0.81	18,655	7459	6.8	220	30	59	59	0.29	0.71	4	2611	1980	101,300	0.4%	Residential
BNG-11–4-1	29.2	45.9	29.2	Heavy	45%	34%	0.68	0.65	5983	6547	9.1	220	35	21	21	0.61	0.56	4	1078	1998	39,600	0.8%	Residential
BNG-11–4-2	23.3	27.0	23.3	Heavy	40%	29%	0.71	0.82	3527	2135	9.4	220	35	17	17	0.37	0.62	4	571	1989	21,325	0.7%	Residential
BNG-11–4-4	40.1	32.8	32.8	Heavy	49%	26%	0.60	0.60	3145	2903	8.8	220	35	14	14	0.60	0.65	4	486	2000	21,000	1.1%	Residential

Building Code	SSR-Y X	SSR	SSR-X	Global Observed Earthquake Damage	Max. axial stress	Aver-age axial stress	Period in Y Direction (s)	Period in X Direction (s)	Base Shear in Y Direction (kN)	Base Shear in X Direction (kN)	f_c (MPa)	f_s (MPa)	Stirrup Spacing (cm)	Number of Columns	Number of Risky Columns	Spectral Acceleration Demand_x (g)	Spectral Acceleration Demand_y (g)	Number of Floors	Total Floor Area (m2)	Year of construction	Total area of vertical elements (cm2)	Longitudinal Reinforcement Ratio (%)	Type of Use
BNG-6–2-8	63.4	23.3	23.3	Heavy	55%	33%	0.42	0.73	1717	1220	5.0	220	25	10	10	0.52	0.74	2	233	1992	14,000	1.7%	Residential
BNG-6-3-1	34.0	25.1	25.1	Heavy	26%	26%	0.54	0.54	5544	4842	8.6	220	40	20	20	0.59	0.67	3	821	1991	37,800	0.5%	Residential
BNG-6-4-2	26.0	18.6	18.6	Heavy	43%	31%	0.68	0.82	11,671	8700	10.4	220	25	42	42	0.43	0.58	4	2021	2001	63,000	1.0%	Residential
BNG-6-4-7	40.5	37.3	37.3	Heavy	45%	32%	0.57	0.67	7007	6468	8.6	220	30	27	27	0.56	0.61	4	1154	1996	46,500	0.5%	Residential
AFY-Ç-02	5.9	36.1	5.9	Heavy	38%	28%	0.71	0.62	1638	1820	9.5	220	35	15	15	0.45	0.41	3	403	2000	15,000	0.9%	Residential
AFY-Ç-03	32.4	17.8	17.8	Heavy	75%	48%	0.66	1.37	1552	695	6.8	220	30	11	11	0.19	0.43	3	358	1991	11,000	1.2%	Residential
AFY-Ç-06	61.7	28.9	28.9	Heavy	37%	22%	0.45	0.71	2115	1442	10.0	220	25	16	16	0.40	0.59	3	359	1990	16,000	0.9%	Residential
AFY-Ç-07	41.6	31.3	31.3	Heavy	40%	27%	0.71	0.81	2659	2340	11.1	220	25	12	12	0.35	0.40	5	662	1975	22,200	0.3%	Residential

Building Code	SSR-Y	SSR-X	Global SSR	Observed Earthquake Damage	Max. axial stress	Aver-age axial stress	Period in Y Direction (s)	Period in X Direction (s)	Base Shear in Y Direction (kN)	Base Shear in X Direction (kN)	f_c (MPa)	f_s (MPa)	Stirrup Spacing (cm)	Num-ber of Columns	Num-ber of Risky Columns	Spectral Acceleration Demand (g)	Spectral Acceleration Demand_y (g)	Num-ber of Floors	Total Floor Area (m2)	Year of construction	Total area of vertical elements (cm2)	Longitudinal Reinforcement Ratio (%)	Type of Use
AFY-Ç-13	15.3	23.3	15.3	Heavy	45%	27%	0.60	0.99	1221	2000	12.7	220	35	12	12	0.29	0.47	4	424	1976	12,450	0.6%	Residential
AFY-ÇO-02	43.7	38.9	38.9	Heavy	70%	46%	1.25	1.27	2627	2549	8.1	220	25	27	27	0.20	0.20	5	1300	1990	35,400	1.0%	Residential
AFY-ÇO-03	29.2	34.8	29.2	Heavy	56%	50%	0.92	0.80	6946	8028	6.6	220	30	44	44	0.33	0.29	5	2397	1997	76,200	0.7%	Residential
AFY-ÇO-05	35.4	32.8	32.8	Heavy	90%	30%	0.56	0.58	1668	1641	8.2	220	30	17	16	0.46	0.47	3	353	2002	15,800	0.7%	Residential
AFY-S-01	22.3	28.9	22.3	Heavy	122%	29%	0.51	0.41	3425	3962	9.4	220	30	19	19	0.64	0.55	4	623	1985	26,350	1.0%	Residential
AFY-Y-01	36.5	40.8	36.5	Heavy	20%	13%	0.53	0.46	4227	4811	9.8	220	45	32	32	0.60	0.52	3	806	1970	64,000	0.5%	Residential
BNG-6-4-3	25.4	19.5	19.5	Collapse	21%	19%	0.49	0.67	4996	4028	19.2	420	30	16	16	0.59	0.73	4	686	2003	19,200	0.6%	Residential
AFY-ÇO-01	17.0	25.1	17.0	Collapse	41%	31%	0.52	0.49	4929	5194	9.8	220	30	22	19	0.52	0.50	4	994	2002	33,000	0.8%	Residential

SSR: Seismic Safety Ratio, f_c: Compressive strength of the existing concrete, f_s: The characteristic yield strength of reinforcement steel.

Stirrup Spacing is observed for reinforced concrete columns at the critical story.

The Longitudinal Reinforcement Ratio paramester is observed or assumed for columns from a representative column.

The Maximum and Average Axial Stress parameters are determined from the critical story.

Spectral Acceleration Demand is determined for considered earthquake events.

Declarations

References

Abrahamson N, Silva W (2008) Summary of the Abrahamson & Silva NGA ground-motion relations. Earthq Spectra. https://doi.org/10.1193/1.2924360

AFAD (2020) Disaster and emergency management presidency, TADAS Ground Motion Database. Ankara, Turkey

Akkar S, Ilki A, Goksu C, and Erdik M (2021) Advances in assessment and modeling of earthquake loss. https://doi.org/10.1007/978-3-030-68813-4

ASCE 41-17 (2017) Seismic Rehabilitation of Existing Buildings, American Society of Civil Engineers ASCE 41-17, United States

Aydinoglu MN (2007) From seismic coefficient to performance based design: 40 years of earthquake engineering from an engineer's viewpoint. Sixth national conference on earthquake engineering, Istanbul, Turkey, 15–41

Aydogdu HH, Demir C, Kahraman T, Ilki A (2023a) Evaluation of rapid seismic safety assessment methods on a substandard reinforced concrete building stock in Istanbul. Structures 56:104962. https://doi.org/10.1016/j.istruc.2023.104962

Aydogdu HH, Demir C, Comert M, Kahraman T, Ilki A (2023b) Structural characteristics of the earthquake-prone building stock in Istanbul and prioritization of existing buildings in terms of seismic risk—a pilot project conducted in Istanbul. J Earthq Eng. https://doi.org/10.1080/13632469.2023.2247481

Bal I, Smyrou E (2016) Simulation of the earthquake-induced collapse of a school building in Turkey in 2011 Van Earthquake. Bull Earthq Eng. https://doi.org/10.1007/s10518-016-0001-x

Beyen K (2018) Hanging wall and footwall effects in the largest reverse-slip earthquake of Turkey, October 23, 2011, MW 7.2 Van Earthquake. Arabian J Sci Eng. https://doi.org/10.1007/s13369-018-3547-x

Bibbee A, Gönenç R, Jacobs S, Konvitz J, and Price R (2000) Economic effects of the 1999 Turkish Earthquakes: an interim report. OECD, Economics Department, OECD Economics Department Working Papers

Binici B, Yakut A, Ozcebe G, Erenler A (2013) Provisions for the seismic risk evaluation of existing RC buildings in turkey under Urban renewal law. Earthq Spectra 31:141208072728004. https://doi.org/10.1193/040513EQS093M

Bommer JJ, Martínez-Pereira A (1999) The effective duration of earthquake strong motion. J Earthq Eng 3(2):127–172. https://doi.org/10.1080/13632469909350343

Bruneau M (2001) Building damage from the Marmara, Turkey earthquake of August 17, 1999. J Seismolog 6:357–377

Cakti E, Safak E, Hancilar U, and Sesetyan K (2019) Updating probable earthquake loss estimates for Istanbul province. Technical Report prepared for Istanbul Metropolitan Municipality (In Turkish)

Celep Z, Erken A, Taskin B, Ilki A (2011) Failures of masonry and concrete buildings during the March 8, 2010 Kovancılar and Palu (Elazığ) Earthquakes in Turkey. Eng Fail Anal 18:868–889. https://doi.org/10.1016/j.engfailanal.2010.11.001

Cimellaro GP, Giovine T, Lopez-Garcia D (2014) Bidirectional pushover analysis of irregular structures. J Struct Eng 140(9):04014059. https://doi.org/10.1061/(asce)st.1943-541x.00

Cosenza E, Del Vecchio C, Di Ludovico M, Dolce M, Moroni C, Prota A, Renzi E (2018) The Italian guidelines for seismic risk classification of constructions: technical principles and validation. Bull Earthq Eng 16:5905–5935. https://doi.org/10.1007/s10518-018-0431-8

Di Ludovico M, Prota A, Moroni C, Manfredi G, Dolce M (2017) Reconstruction process of damaged residential buildings outside historical centres after the L'Aquila earthquake: part II—"heavy damage" reconstruction. Bull Earthq Eng 15(2):693–729. https://doi.org/10.1007/s10518-016-9979-3

Erdik M (2001) Report on 1999 Kocaeli and Düzce (Turkey) Earthquakes. Struct Control Civil Infrastruct Eng 149–186:2001

General Directorate of Mineral Exploration and Research (2003) 1 May 2003 Bingöl Earthquake Evaluation Report. Department of Geology Studies, Ankara, Turkey

Gentile R, Del Vecchio C, Pampanin S, Raffaele D, Uva G (2019) Refinement and validation of the simple lateral mechanism analysis (SLaMA) procedure for RC frames. J Earthq Eng. https://doi.org/10.1080/13632469.2018.1560377

Gurbuz T, Cengiz A, Kolemenoglu S, Demir C, Ilki A (2022) Damages and failures of structures in Izmir (Turkey) during the October 30, 2020 Aegean Sea earthquake. J Earthq Eng. https://doi.org/10.1080/13632469.2022.2086186

Holzer TL, Barka AA, Carver D, Celebi M, Cranswick E, Dawson T, Dieterich JH, Ellsworth WL, Fumal T, Gross JL, Langridge R, Lettis WR, Meremonte M, Mueller C, Olsen RS, Ozel O, Parsons T, Phan LT, Rockwell T, Toprak S (2000) Implications for earthquake risk reduction in the United States from the Kocaeli, Turkey, earthquake of August 17, 1999. US Geol Surv Circular 1193:1–64

Ilki A, Celep Z (2012) Earthquakes, existing buildings and seismic design codes in Turkey. Arab J Sci Eng 37(2):365–380

Ilki A, Comert M, Demir C, Orakcal K, Ulugtekin D, Tapan M, Kumbasar N (2014) Performance based rapid seismic assessment method (PERA) for reinforced concrete frame buildings. Adv Struct Eng 17(3):439–459. https://doi.org/10.1260/1369-4332.17.3.439

Ilki A, and Kumbasar N (2000). Marmara and Duzce earthquakes in Turkey-structural damage. In: ASCE 14th engineering mechanics conference, on CD, Austin, Texas, USA

Ilki A, Halici OF, Comert M, and Demir C (2020) The modified post-earthquake damage assessment methodology for TCIP (TCIP-DAM-2020). In: Advances in assessment and modeling of earthquake loss, eds

Ilki A, Kahraman T, Ozkan S, Aydogdu HH, Demir C, and Comert M (2021a) Seismic risk assessment of building stock in Istanbul. In: ACE2020 14th international congress on advances in civil engineering, Sep 6-8, Istanbul, Turkey. (Keynote lecture)

Ilki A, Halici OF, Kupcu E, Comert M, and Demir C (2021b) Modifications on seismic damage assessment system of TCIP based on reparability. In: 17WCEE, the 17th World Conference on Earthquake Engineering, Sendai, 2020–2021

Inci P, Goksu C, Ilki A, Kumbasar N (2013) Effects of reinforcement corrosion on the performance of RC frame buildings subjected to seismic actions. J Perform Constr Facil 27:683–696. https://doi.org/10.1061/(ASCE)CF.1943-5509.0000378

Mai PM, Spudich P, Boatwright J (2005) Hypocenter locations in finite-source rupture models. Bull Seismol Soc Am 95:965–980. https://doi.org/10.1785/0120040111

Makra K, Rovithis E, Riga E, Raptakis D, Pitilakis K (2021) Amplification features and observed damages in İzmir (Turkey) due to 2020 Samos (Aegean Sea) earthquake: identifying basin effects and design requirements. Bull Earthq Eng 19:4773–4804. https://doi.org/10.1007/s10518-021-01148-3

Marasco S, Zamani Noori A, Domaneschi M, Cimellaro GP (2021) A computational framework for large-scale seismic simulations of residential building stock. Eng Struct 244:112690. https://doi.org/10.1016/j.engstruct.2021.112690

METU (2003) SERU Database Middle East Technical University, Ankara, Turkey. https://seru.metu.edu.tr/

New Zealand Society for Earthquake Engineering (NZSEE) (2017) The seismic assessment of existing buildings—technical guidelines for engineering assessments. Wellington, New Zealand

Ozdemir P, Taskin B, Vatansever C, Sezen A, Ilki A, and Boduroglu H (2002) November 12, 1999 Duzce earthquake: reconnaissance report for the town of Kaynasli. In: 12th European conference on earthquake engineering, on CD, London, UK

Ozmen B (2000) The damage state of the Izmit Bay on 17 August 1999. TDV/DR 010–53, Turkish Earthquake Foundation, p 132

Parsons T, Toda S, Stein RS, Barka A, Dieterich JH (2000) Heightened odds of large earthquakes near Istanbul: an interaction-based probability calculation. Science 288:661–665

Polese M, Gaetani d'Aragona M, Di Ludovico M, Prota A (2018) Sustainable selective mitigation interventions towards effective earthquake risk reduction at the community scale. Sustainability 10(8):2894. https://doi.org/10.3390/su10082894

PROCEQ (2002) User manual for Schmidt Hammer type N-L-NR-LR. Zurich, Switzerland

RBTE (2019) Provisions for the Seismic Risk Evaluation of Existing RC Buildings under Urban Renewal Law, Ministry of Environment and Urbanization, Ankara, Turkey

Scawthorn C, Johnson GS (2000) Preliminary report: Kocaeli (Izmit) earthquake of 17 August 1999. Eng Struct 22:727–745. https://doi.org/10.1016/S0141-0296(99)00106-6

Sextos AG, Kappos AJ, Stylianidis KC (2007) Computer-aided pre- and post-earthquake assessment of buildings involving database compilation, GIS visualization, and mobile data transmission. Comput Aided Civil Infrast Eng 23(1):59–73. https://doi.org/10.1111/j.1467-8667.2007.00513

TSDC (1975) Specification for Structures to be Built in Disaster Areas, Turkish Ministry of Public Works and Settlement, Ankara, Turkey

TSDC (1998) Specification for Structures to be Built in Disaster Areas, Turkish Ministry of Public Works and Settlement, Ankara, Turkey

TSDC (2007) Specification for Structures to be Built in Disaster Areas, Turkish Ministry of Public Works and Settlement, Ankara, Turkey

Tapan M, Cömert M, Demir C, Sayan Y, Orakcal K, Ilki A (2013) Failures of structures during the October 23, 2011 Tabanli (Van) and November 9, 2011 Edremit (Van) earthquakes in Turkey. Eng Failure Anal. https://doi.org/10.1016/j.engfailanal.2013.02.013

TBEC (2018) Turkish Building Earthquake Code, Disaster and emergency management presidency, Ankara, Turkey

Turkish Ministry of Interior Affairs Disaster and Emergency Management Presidency (2018) Earthquake Hazard Map of Turkey, https://tdth.afad.gov.tr/TDTH/userLogin.xhtml. Accessed 20 Dec 2021

Url-1. <https://deprem.afad.gov.tr/tarihteBuAy?id=74>, Accessed 21 March 2020

Url-2. < https://usgs.maps.arcgis.com/apps/webappviewer/index.html?id=8ac19bc334f747e486 550f32837578e1>, Accessed 15 Jan 2022

Url-3. < http://www.koeri.boun.edu.tr/sismo/depremler/onemliler/01mayis2003_bingoldepremi.pdf>, Accessed 20 March 2020

Yakut A, Sucuoğlu H, Binici B, Canbay E, Donmez C, İlki A, Caner A, Celik OC, Ay BÖ (2021) Performance of structures in İzmir after the Samos Island Earthquake. Bull Earthq Eng. https://doi.org/10.1007/s10518-021-01226-6